Chapter 4

Multifunctional hybrid sulfonamides as novel therapeutic agents for Alzheimer's disease

4.1 Introduction

AD is a complex neurodegenerative disorder characterized by cognitive decline and memory deficit. Cholinergic dysfunction and acetylcholinesterase co-localize with amyloid β (Aβ) and enhance its aggregation into insoluble plaques. Histopathologically, AD is indicated by neuritic plaques (NP's) composed of Aβ and neurofibrillary tangles (NFT's). Extracellular accumulation of senile plaques in brain is the central cause of AD.

$A\beta_{42}$ peptide, considered a highly toxic species, undergoes aggregation leading to the formation of protofibrils, oligomers, and completely developed fibrils [59]. Biometals like Fe, Cu and Zn are considered to be involved in the formation of amyloid plaques. Aβ-metal complexes are known inhibitors of Aβ clearance and are involved in the stabilization of the toxic oligomeric state [60]. Moreover, Aβ-metal complexes undergo redox cycle to generate reactive oxygen species (ROS) that lead to neuronal cell death [61]. Therefore, modulating the metal dependent and independent Aβ aggregation is an alluring target for drug design in AD.

Matrix metalloproteinases levels are found to be very low in the healthy human brain. However, injuries and neurodegenerative diseases such as AD are reported to upregulate the levels of MMPs [62-64]. Brkie *et al.,* established a correlation between MMPs and Aβ induced blood-CSF barrier (BCSFB) leakage by measuring the expression of the MMP gene in choroid plexus epithelial tissues (CP) and cerebrospinal fluid (CSF). Aβ oligomer injection to brain leads to an increase in MMP activity. co-treatment of the Aβ oligomers with a non-selective MMP inhibitor, GM6001, via the intracerebroventricular reduced Aβ oligomers-mediated disruption of the BCSFB [65, 66]. MMP-2 and 9 are found to be involved in pathological cascade of AD [67]. However, the role of MMP-9 in the Aβ based neurotoxicity is not clearly understood in case of AD [68].

Although, AChE is the principal cholinesterase in the healthy human brains, a decrease in its activity coupled with an increase of BChE activity has been observed in the cortical regions of

the AD brain [69]. While, BChE is expressed at levels lower than that of AChE in both the hippocampus and neocortex (temporal part), but has been shown that BChE can act as a substitute for AChE by hydrolyzing ACh in several AChE-knockout mice models [70]. The enhance presence of BChE in Aβ/apolipoprotein E(APOE) complexes compounded with plaques leading to neurodegeneration necessiates the development BChE inhibitors [69].

The essential criterion for multi-target drugs is their ability to accomplish high potencies against the selected multiple targets.But is difficult to achieve high potencies against proteins of different families [71]. The commonly used design strategy formultitargeted compounds, is to obtain a hybrid molecule structure by combining distinct pharmacophores of various drugs [72, 73]. Principally, it is essential in this case that the pharmacophores in the compound should retain their individual interactions with respective targets for slowing down or blocking the neurodegenerative processes [74].

Currently approved drugs used in the treatment of AD consist of the Cholinesterase inhibitors such as donepezil (DNP), galantamine and rivastigmine. A fourth drug memantine, an NMDA antagonist is used both in monotherapy and as a part of the combination therapy with the AChEI's [75]. However, the complex pathophysiology of AD requires development of multifunctional ligands to slice through the multifactorial pathways involved in AD [76]. Several research groups have developed potent multitargeted compounds and achieved nanomolar range activities against various targets such as Aβ, β-Secretase, 5-HT_6, AchE and BChE [76-78]. Earlier, we reported the design, synthesis and evaluation of piperazinediones, as multifunctional therapeutic ligands for AD [79, 80].

4.2 Materials and methods

4.2.1 Rationale of drug design & in-silico optimization

The drug design strategy in the study is further combined with modern in-silico techniques to develop quinoline/indole-based inhibitors. Quinolines and indoles cause weak metal chelation and thus are suitable nuclei for the inhibition of metal induced Aβ aggregation and MMPs triggered abnormalities in AD. Biphenyl substitutions were incorporated in most of the designed compounds to increase their accessibility to various sub-sites of MMP-2 and 9. Aromatic and heterocyclic groups connected with two or three carbon linkers are the established pharmacophores for AChE inhibition. This validated hypothesis encouraged us to screen the molecules initially against AChE, by in-silico methods, followed by in-vitro experiments. The molecules produced decent docking scores on Aβ protein. The Aβ anti-aggregative property of the compounds was experimentally determined using $A\beta_{1-42}$ induced intracerebroventricular (ICV) rat model of AD.

The pharmacophoric features of centrally acting cholinesterase inhibitors viz. DNP, metal chelators and MMP inhibitors were identified and used in a hybrid pharmacophore-based approach to design a library of compounds. Docking studies were performed for the compounds to detect the various functional groups and fragments likely involved in making the crucial interactions with the active sites of AChE and MMP-2. Novel molecules showing the best interactions in in-silico were then synthesized and screened for AChE and MMP-2 inhibition among other parameters.

4.2.2 Virtual screening of commercial and non-commercial databases

Structure-based virtual screening was conducted against AChE and MMP-2 using the ZINC and ASINEX databases (PDB: 4EY7, 1HOV). Using PyRx, virtual screening was carried out. Protein preparation and receptor grid creation were applied to the proteins 4EY7 and 1HOV.

The following criteria were used to construct the internal tiny fragment library: Lipophilic groups, a molecular weight of less than 250 Da, and an equivalent number of aromatic rings, or more, are required. Using the Glide XP module of Schrödinger Maestro 2018, a number of internal pieces were docked in the preliminary stage. Through polar contact, fragments demonstrated interactions with residues of the catalytic active site (CAS) of AChE. Consequently, the fragments showing good docking poses were selected and used prototypes for the de novo design of molecules.

The desired outcome of a structure-based virtual screen (SBVS) campaign is a hit or small set of hits with activities against the target in micro molar or nano molar ranges. Important considerations for a successful SBVS project include the selection of a suitable database of compounds. The central step in SBVS is the docking of the candidate ligands to the target. Majority of small molecules interact with their targets through noncovalent binding, molecular docking programs are utilized to simulate the process of ligand and target interactions to form a noncovalent complex, revealing the steric and electrostatic complementarity between them. Docking programs predict both a binding mode – the position and orientation of the ligand relative to the target – and a score – the quantitative measure of how well the ligand fits into and interacts with the target binding site.

While virtual screening encompasses the wider notion of screening an extensive compound library, the specific techniques employed in a VS project include SP docking and XP docking. VS is a high-throughput computational technique designed to rapidly sort through a large number of ligand libraries against a target protein using scoring functions or filters in order to find possible drug candidates that are most likely to bind to a target protein, allowing for the final candidate to be experimentally evaluated.

The terms SP and XP are the frequently used molecular docking methods, particularly in the context of software such as Autodock. The two techniques refer to the variation in the levels of accuracy and computational intensity in the docking calculations.

SP docking typically conducts a constrained search of the conformational space of the ligand. Although, it is a faster method, it is less exhaustive may not capture every binding mode. Reduced computational demands makes it suitable for scenarios with constrained computational resources as well as for high-throughput virtual screening. On the other hand, XP docking is a precise and computationally intensive method that uses advanced scoring functions to explore the ligand's conformational space in greater detail. It considers factors like solvation effects, entropic contributions, and force fields, resulting in more accurate predictions of binding affinities. XP docking also involves thorough examination of the ligand's conformational space, considering multiple conformations and energy states. Despite its computational resources, it is often used when higher accuracy is critical, even at the cost of increased computational time.

4.2.3 Extra precision molecular docking

The hit molecules acquired from off-target virtual screening and filtering steps were additionally docked against AChE and MMP-2 (PDB: 4EY7, 1HOV) using Maestro's Glide XP (extra precision) mode in order to study the various ligand poses of the molecules so as to eliminate the false positives in order to improve the correlation between good score and good pose

4.2.4 Chemistry

Chemicals and reagents were procured from Spectrochem, Sigma-Aldrich, Alfa Aesar and Avra. The progress of reactions was examined by thin layer chromatography (TLC) on precoated silica gel 60 F254 plates (Merck KGaA), using ultraviolet light (254 nm) and iodine vapors for visualization of spots. Synthesized compounds were purified on silica gel (60-120 mesh size). Automated melting point apparatus (Bamstead Electrothermal, UK) was used to determine the melting point of compounds. The ^{1}H NMR and ^{13}C NMR spectra were recorded on Bruker Advance, 500 MHz spectrometer in DMSO-d_6 and $CDCl_3$. Chemical shift and coupling constant (*J*) were measured in ppm (δ) and Hz. Mass analysis was performed on LC-MS spectrometer model Q-ToF Micro Waters Mass spectra with EI ion source and FTIR spectra was recorded on Bruker ALPHA-T (Germany) ATR /FT-IR instrument. Purity of the synthesized compounds was established by HPLC (Shimadzu LC 20 AD). Isocratic mobile phase was delivered by quaternary pumps with flow rate of 1mL /min. The mobile phase composition was phase A (acetonitrile) and phase B (methanol) in ratio of 0.5:0.5. 20 µL samples were injected into the HPLC column. SPD10AVP detector was used at 365 nm for the detection of the compounds. CLC C_{18} column (5µm, 25 cm x 4.6mm i.d, with CLC ODS, 4cm x 4.6 mm. i.d as guard column) was used for purification.

4.2.5 Scheme I- Synthesis of p-substituted benzene alkanoic amide derivatives

Step I: Synthesis of sulfonamides using different aminoacids

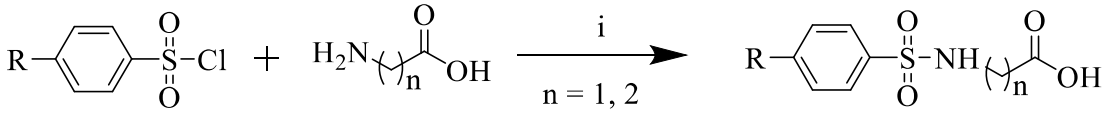

1-7 **8-9** **10-17**

Comp. No. 1, 2, 3, 4, 5, 6, 7
R. H, F, Cl, FPh, Ph, ClPh, OCH_3

Reagents and conditions: i) Na_2CO_3/K_2CO_3, Water-Acetone mixture (1:1).

Step-2: Synthesis *of* 3-((4'-substituted-[1,1'-aryl])-4-sulfonamido) alkanoyl chloride.

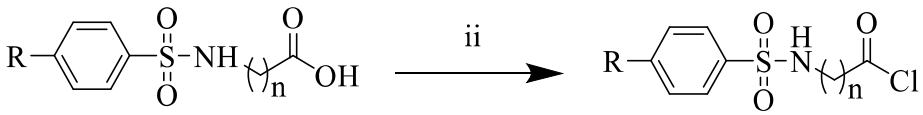

10-17 **18-26**

Comp. No. 18, 19, 20, 21, 22, 23, 24, 25 26
R. H, F, Cl, FPh, Ph, ClPh, OCH_3, OCH_3 FPh
n. 1, 1, 2, 1, 2, 2, 1, 2 2

Reagents and conditions: ii) $SOCl_2$, 75 ºC.

Step-3: Synthesis of p-substituted benzene alkanoic amide.

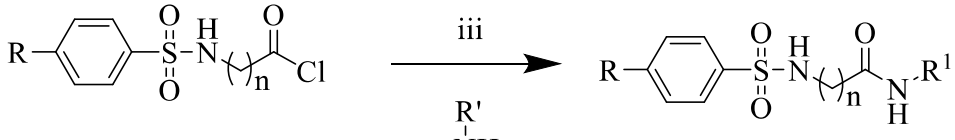

18-26 **27-30** **31-46**

Comp. No. 27, 28 29 30
R'.

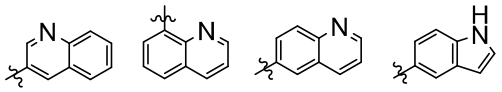

Reagents and conditions: iii) Amine, dry THF, Triethylamine.

4.2.5.1 General method for the synthesis of *p-substituted-phenyl sulphonyl alkanoic acid* (10-17)

Compounds (1-7) were purchased from Sigma-Aldrich and amino acids (8-9) were procured from Avra chemicals, India. The substituted aromatic sulphonyl chlorides (1-7) (9.6 mmol, 1 equivalent) and amino acids (8-9) (9.6 mmol, 1 equivalent) were dissolved in the acetone, water mixture (1:1, 2 mL). The mixture was stirred with sodium bicarbonate (28.8 mmol, 3 equivalents) at room temperature (rt) for 24 h. The reaction was monitored by TLC using ethyl acetate and methanol (8:2) as the mobile phase. The acetone was evaporated under reduced pressure and reaction mixture was neutralized with 1N HCl to get the product. The product was filtered and recrystallized with methanol to get the pure compound.

4.2.5.2 General method for synthesis of 2/3-(substituted biphenyl/ phenyl sulfonamido) ethanoic/propanoic acid chloride (18-26)

Different 2/3-(substituted biphenyl/phenyl sulfonamide) ethanoic/propanoic (4.7 mmol) acids (10-17) were treated with thionyl chloride (93.0 mmol, 20 equivalent) and the reaction mixture was stirred at 75 ºC for 45 min in a nitrogen environment. The final reaction mixture obtained, after 45 min, was dried by vacuum rotary evaporator to get the chlorides of compounds 10-17. The corresponding acid chlorides then obtained were immediately used for the next step of the reaction.

4.2.5.3 General method for synthesis of Novel 3-((4-substituted) sulfonamido)-N-(indole/quinolin-3/6/8-yl) ethan/propanamide (31-46)

Compounds 27-30 were purchased from Sigma-Aldrich. The 2/3-(substituted biphenyl/phenyl sulfonamido) ethanoic/propanoic acid chlorides (18-26) (4.6 mmol, 1 equivalent) were dissolved in dry THF (5 mL) and treated with different amino indoles/quinolines (27-30) (4.6 mmol, 1 equivalent) and triethylamine (9.2 mmol, 2 equivalent) to get the crude compounds. The compounds obtained were extracted with ethyl acetate, dried and washed with 5% ethyl acetate, hexane mixture. The compounds were finally purified by column chromatography to

obtain the final pure product (31-46). Further the HPLC was performed to check the purity of all synthesized compounds and whereby, the compounds were found to be more than 99% pure.

2-(phenylsulfonamido)-N-(quinolin-3-yl)acetamide (**31**): It was synthesized as per general procedure mentioned in section (4.1.3) using (phenylsulfonyl)glycinoyl chloride (**18**) (1.07 g) and quinolin-3-amine (**27**) (0.66 gm) to get compound **31** as light brown powder, yield 70%; mp 120-122 ºC; FTIR (KBr) cm^{-1}: 3413 (NH-str.), 2875 (Ar-str.), 1647 (C=O-str.), 1123 (SO_2-str.); ^{1}H NMR (500 MHz, DMSO-d_6) δ 8.12 (t, 1H, *J* = 5 Hz, quinolinyl-C_2), 8.05 (s, 1H, -NH), 7.92-7.87 (m, 1H, quinolinyl-C_4), 7.82 (d, 1H, *J* = 5, quinolinyl-C_8), 7.72 (t, 1H, *J* = 5 Hz, quinolinyl-C_7), 7.68 (d, 2H, *J* = 10 Hz, phenyl-C_2, C_6), 7.63 (s, 1H, phenyl-C_4), 7.56 (s, 1H, phenyl-C_3), 7.54 (s, 1H, phenyl-C_4), 7.52-7.50 (m, 2H, quinolinyl-C_5, C_6), 3.68 (s, 1H, sulfonamide-NH), 3.46 (s, 1H, acetamide-CH_2); ^{13}C NMR (125 MHz, DMSO-d_6) δ 168.21 (acetamide-CO), 157.85 (quinolinyl-C_2), 155.76 (phenyl-C_1), 155.27 (quinolinyl-C_3), 145.03 (quinolinyl bridge-C_{8a}), 142.24 (quinolinyl-C_4), 141.85 (quinolinyl-C_8), 130.95 (quinolinyl-C_7), 130.24 (quinolinyl-C_6), 129.41 (quinolinyl bridge-C_{4a}), 128.74 (quinolinyl-C_5), 127.58 (phenyl-C_2), 126.59 (phenyl-C_6) 125.45 (phenyl-C_3), 124.94 (phenyl-C_4), 124.27 (biphenyl-C_3), 123.74 (biphenyl-C_5), 49.42 (acetamide-CH_2); MS (ESI): *m/z* found 342.44 [M^+]; calculated for $C_{17}H_{15}N_3O_3S$ 341.08.

2-((4-fluorophenyl)sulfonamido)-N-(quinolin-3-yl)acetamide (**32**): Synthesized as per general procedure mentioned in section (4.1.3) using ((4-fluorophenyl) sulfonyl) glycinoyl chloride (**19**) (1.15 g) and quinolin-3-amine (**27**) (0.66 gm) to get compound **32** as light brown powder, yield 75%; mp 135-137 ºC; FTIR (KBr) cm^{-1}: 3410 (NH-str.), 2875 (Ar-str.), 1645 (C=O-str.), 1118 (SO_2-str.); ^{1}H NMR (500 MHz, DMSO-d_6) δ 8.54 (s, 1H, -NH), 8.18 (t, 1H, *J* = 5 Hz, quinolinyl-C_2), 7.96-7.91 (m, 1H, quinolinyl-C_4), 7.85 (d, 1H, *J* = 5 Hz, quinolinyl-C_8), 7.80-7.78 (m, 3H, fluorophenyl-C_2, C_6 and quinolinyl-C_7), 7.67-7.64 (m, 4H, fluorophenyl-C_3, C_5 and quinolinyl-C_5, C_6), 3.79 (s, 1H, sulfonamide-NH), 3.62 (s, 2H, acetamide-CH_2); ^{13}C NMR

(125 MHz, DMSO-d_6) δ 166.54 (fluorophenyl-C_4), 165.00 (acetamide-CO), 163.47 (quinolinyl-C_2), 146.24 (fluorophenyl-C_1), 144.57 (quinolinyl bridge-C_{8a}), 139.84 (quinolinyl-C_3), 135.82 (fluorophenyl-C_3, C_5), 133.74 (fluorophenyl-C_2, C_6), 131.14 (quinolinyl-C_8), 129.47 (quinolinyl-C_4), 128.41 (quinolinyl bridge-C_{4a}), 127.74 (quinolinyl-C_7), 125.81 (quinolinyl-C_6), 125.28 (quinolinyl-C_5), 48.54 (acetamide-CH_2); MS (ESI): *m/z* found 360.41 [M^+]; calculated for $C_{17}H_{14}FN_3O_3S$ 359.07.

3-((4-chlorophenyl)sulfonamido)-N-(quinolin-3-yl)propanamide (**33**): The compound was synthesized as per general procedure mentioned in section (4.1.3) using 3-((4-chlorophenyl)sulfonamido)propanoyl chloride (**20**) (1.29 g) and quinolin-3-amine (**27**) (0.66 gm) to get compound **33** as buff white solid, yield 62 %; mp 162-164ºC; FTIR (KBr) cm^{-1}: 3395 (NH-str.), 2840 (Ar-str.), 1684 (C=O-str.), 1104 (SO_2-str.); ^{1}H NMR (500 MHz, DMSO-d_6) δ 10.42 (s, 1H, -NH), 8.88 (s, 1H, quinolinyl-C_2), 8.64 (s, 1H, quinolinyl-C_4), 7.95-7.89 (m, 3H, quinolinyl-C_8, chlorophenyl-C_3, C_5), 7.83-7.79 (m, 2H, chlorophenyl-C_2, C_6), 7.69-7.62 (m, 2H, quinolinyl-C_5, C_7), 7.58 (t, 1H, J_1 = 10, J_2 = 5 Hz, quinolinyl-C_6), 3.14 (q, 2H, J_1 = 5, J_2 = 10, J_3 = 5 Hz, propanamide-CH_2), 2.96 (s, 1H, sulfonamide-NH), 2.60 (t, 2H, J_1, J_2 = 5 Hz, propanamide-$COCH_2$); ^{13}C NMR (125 MHz, DMSO-d_6) δ 171.10 (acetamide-CO), 165.74 (chlorophenyl-C_4), 161.52 (quinolinyl-C_2), 142.47 (chlorophenyl-C_1), 141.10 (quinolinyl bridge-C_{8a}), 137.14 (quinolinyl-C_3), 135.43 (chlorophenyl-C_3, C_5), 131.48 (chlorophenyl-C_2, C_6), 129.87 (quinolinyl-C_8), 12.50 (quinolinyl-C_4), 128.62 (quinolinyl bridge-C_{4a}), 127.41 (quinolinyl-C_7), 126.04 (quinolinyl-C_6), 125.74 (quinolinyl-C_5), 37.84 (propanamide-$NHCH_2$), 34.51 (propanamide-CH_2); MS (ESI): *m/z* found 390.47 [M^+]; calculated for $C_{18}H_{16}ClN_3O_3S$ 389.06.

2-((4'-fluoro-[1,1'-biphenyl])-4-sulfonamido)-N-(quinolin-3-yl)acetamide (**34**): It was synthesized as per general procedure mentioned in section (4.1.3) using ((4'-fluoro-[1,1'-biphenyl]-4-yl)sulfonyl)glycinoyl chloride (**21**) (1.50 g) and quinolin-3-amine (**27**) (0.66 gm)

to get compound **34** as buff white solid, yield 67%; mp 190-192 ºC; FTIR (KBr) cm^{-1}: 3415 (NH-str.), 2858 (Ar-str.), 1657 (C=O-str.), 1120 (SO_2-str.); ^{1}H NMR (500 MHz, DMSO-d_6) δ 10.44 (s, 1H, -NH), 8.82 (s, 1H, quinolinyl-C_2), 8.52 (s, 1H, quinolinyl-C_4), 8.27 (s, 1H, sulfonamide-NH), 7.94-7.91 (m, 3H, fluorophenyl-C_3, C_5, quinolinyl-C_8), 7.86-7.84 (m, 3H, phenyl-C_2, C_6 and quinolinyl-C_7), 7.66-7.63 (m, 3H, fluorophenyl-C_2, C_6 and quinolinyl-C_5), 7.56 (t, 1H, J_1 = 5, J_2 = 10 Hz, quinolinyl-C_6), 7.50 (d, 2H, J = 10 Hz, phenyl-C_3, C_5), 3.81 (s, 2H, acetamide-CH_2); ^{13}C NMR (125 MHz, DMSO-d_6) δ 163.41 (fluorophenyl-C_4), 162.74 (acetamide-CO), 158.77 (quinolinyl-C_2), 145.54 (phenyl-C_1), 143.75 (quinolinyl bridge-C_{8a}), 141.53 (quinolinyl-C_3), 135.38 (fluorophenyl-C_1, C_3, C_5), 132.84 (phenyl-C_2, C_4, C_6), 129.88 (quinolinyl-C_8), 129.57 (quinolinyl-C_4), 129.10 (quinolinyl bridge-C_{4a}), 128.57 (quinolinyl-C_7), 128.31 (quinolinyl-C_6), 127.54 (quinolinyl-C_5), 127.28 (fluorophenyl-C_2, C_6), 125.62 (phenyl-C_3, C_5), 45.38 (acetamide-CH_2); MS (ESI): *m/z* found 436.87 [M^+]; calculated for $C_{23}H_{18}FN_3O_3S$ 435.11.

3-([1,1'-biphenyl]-4-sulfonamido)-N-(quinolin-3-yl)propanamide (**35**): The compound was synthesized as per general procedure mentioned in section (4.1.3) using 3-([1,1'-biphenyl]-4-sulfonamido)propanoyl chloride (**22**) (1.48 g) and quinolin-3-amine (**27**) (0.66 gm) to get compound **35** as buff white solid, yield 60; mp 185-188 ºC; FTIR (KBr) cm^{-1}: 3356 (NH-str.), 2872 (Ar-str.), 1700 (C=O-str.), 1142 (SO_2-str.); ^{1}H NMR (500 MHz, DMSO-d_6) δ 10.45 (s, 1H, -NH), 8.89 (s, 1H, quinolinyl-C_2), 8.66 (s, 1H, quinolinyl-C_4), 8.28 (s, 1H, sulfonamide-NH), 7.95-7.84 (m, 6H, biphenyl-C_2, C_3, C_5, C_6, $C_{3'}$, quinolinyl-C_8), 7.76-7.71 (m, 2H, biphenyl-$C_{2'}$, $C_{6'}$), 7.66-7.62 (m, 1H, quinolinyl-C_7), 7.58-7.54 (m, 1H, quinolinyl-C_6), 7.52 (t, 2H, J_1 = 10, J_2 = 5 Hz, biphenyl-$C_{4'}$, $C_{5'}$), 7.45-7.42 (m, 1H, quinolinyl-C_5), 3.17 (q, 2H, J_1 = 5, J_2 = 5, J_3 = 10 Hz, propanamide-CH_2), 2.64 (t, J_1 = 5, J_2 = 5, 2H, propanamide-$COCH_2$); ^{13}C NMR (125 MHz, DMSO-d_6) δ 168.57 (acetamide-CO), 158.87 (quinolinyl-C_2), 156.85 (biphenyl-C_1), 155.45 (quinolinyl-C_3), 146.27 (quinolinyl bridge-C_{8a}), 143.28 (quinolinyl-C_4),

141.85 (quinolinyl-C_8), 132.57 (quinolinyl-C_7), 130.74 (quinolinyl-C_6), 129.57 (quinolinyl bridge-C_{4a}), 128.65 (quinolinyl-C_5), 127.85 (biphenyl-C_2, C_6), 127.84 (biphenyl-$C_{1'}$), 125.75 (biphenyl-C_3, C_5), 125.24 (biphenyl-$C_{2'}$, $C_{6'}$), 124.54 (biphenyl-$C_{3'}$), 123.84 (biphenyl-$C_{4'}$), 123.62 (biphenyl-C_4), 122.58 (biphenyl-$C_{5'}$), 50.84 (propanamide-$NHCH_2$), 48.57 (propanamide-CH_2); MS (ESI): *m/z* found 432.48 [M^+]; calculated for $C_{24}H_{21}N_3O_3S$ 431.13.

3-((4'-chloro-[1,1'-biphenyl])-4-sulfonamido)-N-(quinolin-3-yl)propanamide (**36**): This was synthesized as per general procedure mentioned in section (4.1.3) using 3-((4'-chloro-[1,1'-biphenyl])-4-sulfonamido)propanoyl chloride (**23**) (1.64 g) and quinolin-3-amine (**27**) (0.66 gm) to get compound **36** as white solid, yield 52%; mp 190-193ºC; FTIR (KBr) cm^{-1}: 3367 (NH-str.), 2887 (Ar-str.), 1705 (C=O-str.), 1147 (SO_2-str.); ^{1}H NMR (500 MHz, DMSO-d_6) δ 10.45 (s, 1H, -NH), 8.88 (d, 2H, *J* = 5Hz, chlorophenyl-C_3, C_5), 8.70 (s, 1H, quinolinyl-C_2), 8.62 (d, 2H, *J* = 5Hz, phenyl-C_2, C_6), 8.53 (s, 1H, quinolinyl-C_4), 8.10 (s, 1H, sulfonamide-NH), 7.95 (d, 2H, *J* = 5Hz, chlorophenyl-C_2, C_6), 7.86-7.82 (m, 1H, quinolinyl-C_8), 7.78-7.74 (m, 1H, quinolinyl-C_5), 7.63 (t, 1H, J_1 = 10, J_2 = 5 Hz, quinolinyl-C_7), 7.54-7.50 (m, 3H, phenyl-C_3, C_5, quinolinyl-C_6), 3.35 (q, 2H, J_1 = 5, J_2 = 5, J_3 = 10 Hz, propanamide-CH_2), 2.79 (t, 2H, J_1 = 5, J_2 = 5, propanamide-$COCH_2$); ^{13}C NMR (125 MHz, DMSO-d_6) δ 172.42 (acetamide-CO), 160.24 (chlorophenyl-C_4), 159.53 (quinolinyl-C_2), 157.57 (phenyl-C_1), 156.85 (chlorophenyl-C_3, C_5), 156.22 (chlorophenyl-C_2, C_6), 155.79 (quinolinyl-C_3), 148.52 (quinolinyl bridge-C_{8a}), 145.44 (quinolinyl-C_4), 144.47 (phenyl-C_2, C_6), 142.74 (quinolinyl-C_8), 134.75 (quinolinyl-C_7), 132.57 (quinolinyl-C_6), 130.74 (quinolinyl bridge-C_{4a}), 129.74 (quinolinyl-C_5), 128.48 (chlorophenyl-C_1), 127.28 (phenyl-C_3, C_5), 126.74 (phenyl-C_4), 52.57 (propanamide-$NHCH_2$), 59.27 (propanamide-CH_2); MS (ESI): *m/z* found 466.72 [M^+]; calculated for $C_{24}H_{20}ClN_3O_3S$ 465.09.

2-((4-methoxyphenyl)sulfonamido)-N-(quinolin-8-yl)acetamide (**37**): Synthesized as per general procedure mentioned in section (4.1.3) using ((4-methoxyphenyl) sulfonyl) glycinoyl

chloride (**24**) (1.67 g) and quinolin-8-amine (**28**) (0.66 gm) to get compound **37** as buff white powder, yield 63%; mp 180-182 ºC; FTIR (KBr) cm^{-1}: 3380 (NH-str.), 2772 (Ar-str.), 1710 (C=O-str.), 1104 (SO_2-str.); ^{1}H NMR (500 MHz, DMSO-d_6) δ 10.64 (s, 1H, -NH), 8.96 (d, 1H, J = 5 Hz, quinolinyl-C_2), 8.62 (d, 1H, J = 10 Hz quinolinyl-C_7), 8.44 (d, 1H, J = 5 Hz, quinolinyl-C_4), 7.82 (d, 2H, J = 10 Hz, methoxyphenyl-C_2, C_6), 7.71-7.66 (m, 2H, methoxyphenyl-C_3, C_5), 7.61 (t, 1H, J_1 = 10, J_2 = 5 Hz, quinolinyl-C_3), 7.16-7.04 (m, 2H, quinolinyl-C_5, C_6), 3.87 (s, 1H, sulfonamide-NH), 3.80 (s, 3H, methoxyphenyl-CH_3), 3.73 (s, 2H, acetamide-CH_2); ^{13}C NMR (125 MHz, DMSO-d_6) δ 167.41 (acetamide-CO), 164.71 (quinolinyl-C_2), 152.42 (methoxyphenyl-C_4), 144.34 (quinolinyl-C_8), 143.84 (methoxyphenyl-C_1), 141.35 (quinolinyl bridge-C_{8a}), 134.71 (methoxyphenyl-C_2, C_6), 133.42 (methoxyphenyl-C_3, C_5), 131.14 (quinolinyl-C_4), 130.54 (quinolinyl-C_7), 128.71 (quinolinyl-C_3), 125.82 (quinolinyl-C_5), 123.52 (quinolinyl-C_6), 120.34 (quinolinyl bridge-C_{4a}), 60.34 (methoxyphenyl-CH_3), 47.58 (acetamide-CH_2); MS (ESI): *m/z* found 372.72 [M^+]; calculated for $C_{18}H_{17}N_3O_4S$ 371.09.

3-((4-methoxyphenyl)sulfonamido)-N-(quinolin-8-yl)propanamide (**38**): This was synthesized as per general procedure mentioned in section (4.1.3) using 3-((4-methoxyphenyl)sulfonamido)propanoyl chloride (**25**) (1.27 g) and quinolin-8-amine (**28**) (0.66 gm) to get compound **38** as buff white powder, yield 65%; mp 175-177 ºC; FTIR (KBr) cm^{-1}: 3375 (NH-str.), 27725 (Ar-str.), 1701 (C=O-str.), 1120 (SO_2-str.); ^{1}H NMR (500 MHz, DMSO-d_6) δ 10.51 (s, 1H, -NH), 8.87 (d, 1H, J = 5 Hz, quinolinyl-C_2), 8.54 (d, 1H, J = 10 Hz quinolinyl-C_7), 8.42 (d, 1H, J = 5 Hz, quinolinyl-C_4), 7.80 (d, 2H, J = 10 Hz, methoxyphenyl-C_2, C_6), 7.70-7.64 (m, 2H, methoxyphenyl-C_3, C_5), 7.63 (t, 1H, J_1 = 10, J_2 = 5 Hz, quinolinyl-C_3), 7.12-7.00 (m, 2H, quinolinyl-C_5, C_6), 3.27 (q, 2H, J_1 = 5, J_2 = 10, J_3 = 5 Hz, propanamide-CH_2), 2.91 (s, 1H, sulfonamide-NH), 2.71 (t, 2H, J_1, J_2 = 5 Hz, propanamide-$COCH_2$); ^{13}C NMR (125 MHz, DMSO-d_6) δ 167.80 (acetamide-CO), 164.54 (quinolinyl-C_2), 152.25

(methoxyphenyl-C_4), 144.24 (quinolinyl-C_8), 143.74 (methoxyphenyl-C_1), 141.27 (quinolinyl bridge-C_{8a}), 134.54 (methoxyphenyl-C_2, C_6), 133.25 (methoxyphenyl-C_3, C_5), 131.24 (quinolinyl-C_4), 130.36 (quinolinyl-C_7), 128.58 (quinolinyl-C_3), 125.57 (quinolinyl-C_5), 123.36 (quinolinyl-C_6), 120.28 (quinolinyl bridge-C_{4a}), 60.54 (methoxyphenyl-CH_3), 38.47 (propanamide-$NHCH_2$), 36.74 (propanamide-CH_2); MS (ESI): *m/z* found 386.31 [M^+]; calculated for $C_{19}H_{19}N_3O_4S$ 385.11.

2-((4'-fluoro-[1,1'-biphenyl])-4-sulfonamido)-N-(quinolin-8-yl)acetamide (**39**): This compound was synthesized as per general procedure mentioned in section (4.1.3) using ((4'-fluoro-[1,1'-biphenyl]-4-yl)sulfonyl)glycinoyl chloride (**21**) (1.5 g) and quinolin-8-amine (**28**) (0.66 gm) to get compound **39** as white powder, yield 62%; mp 183-185 ºC; FTIR (KBr) cm^{-1}: 3424 (NH-str.), 2863 (Ar-str.), 1687 (C=O-str.), 1148 (SO_2-str.); ^{1}H NMR (500 MHz, DMSO-d_6) δ 10.71 (s, 1H, -NH), 8.96 (s, 1H, sulfonamide-NH), 8.61 (d, 1H, *J* = 10 Hz, quinolinyl-C_2), 8.42 (d, 1H, *J* = 5 Hz, quinolinyl-C_7), 7.94-7.83 (m, 5H, fluorophenyl-C_3, C_5, phenyl-C_2, C_6, quinolinyl-C_3), 7.78 (d, 1H, quinolinyl-C_4), 7.71 (d, 2H, *J* = 10 Hz, fluorophenyl-C_2, C_6), 7.67-7.64 (m, 1H, quinolinyl-C_6), 7.58-7.55 (m, 3H, phenyl-C_3, C_5, quinolinyl-C_5), 3.80 (s, 2H, acetamide-CH_2); ^{13}C NMR (125 MHz, DMSO-d_6) δ 164.85 (fluorophenyl-C_4), 163.87 (acetamide-CO), 158.54 (quinolinyl-C_2), 146.68 (phenyl-C_1), 143.85 (quinolinyl bridge-C_{8a}), 141.74 (quinolinyl-C_3), 135.98 (fluorophenyl-C_1, C_3, C_5), 132.84 (phenyl-C_2, C_4, C_6), 130.57 (quinolinyl-C_8), 129.84 (quinolinyl-C_4), 129.30 (quinolinyl bridge-C_{4a}), 128.55 (quinolinyl-C_7), 128.74 (quinolinyl-C_6), 127.24 (quinolinyl-C_5), 126.78 (fluorophenyl-C_2, C_6), 125.14 (phenyl-C_3, C_5), 46.80 (acetamide-CH_2); MS (ESI): *m/z* found 436.62 [M^+]; calculated for $C_{23}H_{18}FN_3O_3S$ 435.11.

3-([1,1'-biphenyl]-4-sulfonamido)-N-(quinolin-8-yl)propanamide (**40**): It was synthesized as per general procedure mentioned in section (4.1.3) using 3-([1,1'-biphenyl]-4-sulfonamido)propanoyl chloride (**22**) (1.48 g) and quinolin-8-amine (**28**) (0.66 gm) to get

compound **40** as pinkish white solid, yield 55%; mp 183-185 ºC; FTIR (KBr) cm^{-1}: 3359 (NH-str.), 2875 (Ar-str.), 1711 (C=O-str.), 1146 (SO_2-str.); ^1H NMR (500 MHz, DMSO-d_6) δ 9.28 (s, 1H, -NH), 8.78 (d, 1H, *J* = 5 Hz, quinolinyl-C_2), 8.11 (d, 1H, *J* = 10 Hz, quinolinyl-C_7), 7.98 (d, 2H, *J* = 10 Hz, biphenyl-C_2, C_6), 7.88-7.87 (m, 1H, quinolinyl-C_4), 7.57 (d, 2H, *J* = 5 Hz, biphenyl-$C_{2'}$, $C_{6'}$), 7.49-7.46 (m, 4H, biphenyl-$C_{3'}$, $C_{5'}$, quinolinyl-C_3, C_5), 7.44-7.34 (m, 4H, quinolinyl-C_6, biphenyl-C_3, C_5, $C_{4'}$), 3.20 (t, 2H, J_1 = 5, J_2 = 5 Hz, propanamide-CH_2), 2.68 (t, 2H, J_1 = 5, J_2 = 5, propanamide-$COCH_2$); ^{13}C NMR (125 MHz, DMSO-d_6) δ 169.25 (acetamide-CO), 159.55 (quinolinyl-C_2), 156.17 (biphenyl-C_1), 155.44 (quinolinyl-C_3), 146.41 (quinolinyl bridge-C_{8a}), 143.41 (quinolinyl-C_4), 142.04 (quinolinyl-C_8), 132.47 (quinolinyl-C_7), 130.54 (quinolinyl-C_6), 129.61 (quinolinyl bridge-C_{4a}), 128.55 (quinolinyl-C_5), 127.85 (biphenyl-$C_{1'}$), 127.74 (biphenyl-C_2, C_6), 126.24 (biphenyl-C_4) 125.84 (biphenyl-C_3, C_5), 125.61 (biphenyl-$C_{2'}$, $C_{6'}$), 124.64 (biphenyl-$C_{3'}$), 123.74 (biphenyl-$C_{4'}$), 123.84 (biphenyl-$C_{5'}$), 50.45 (propanamide-$NHCH_2$), 48.74 (propanamide-CH_2); MS (ESI): *m/z* found 432.74 [M^+]; calculated for $C_{24}H_{21}N_3O_3S$ 431.13.

3-((4'-chloro-[1,1'-biphenyl])-4-sulfonamido)-N-(quinolin-8-yl)propanamide (**41**): The compound was synthesized as per general procedure mentioned in section (4.1.3) using 3-((4'-chloro-[1,1'-biphenyl])-4-sulfonamido)propanoyl chloride (**23**) (1.64 g) and quinolin-8-amine (**28**) (0.66 gm) to get compound **41** as white solid powder, yield 52%; mp 187-189 ºC; FTIR (KBr) cm^{-1}: 3371 (NH-str.), 2880 (Ar-str.), 1708 (C=O-str.), 1152 (SO_2-str.); ^1H NMR (500 MHz, DMSO-d_6) δ 10.36 (s, 1H, -NH), 8.84 (d, 2H, *J* = 5Hz, chlorophenyl-C_3, C_5), 8.72 (s, 1H, quinolinyl-C_2), 8.64 (d, 2H, *J* = 5Hz, phenyl-C_2, C_6), 8.56 (s, 1H, quinolinyl-C_7), 8.07 (s, 1H, sulfonamide-NH), 7.92 (d, 2H, *J* = 5Hz, chlorophenyl-C_2, C_6), 7.88-7.84 (m, 1H, quinolinyl-C_6), 7.76-7.72 (m, 2H, quinolinyl-C_4, C_5), 7.64 (t, 1H, J_1 = 10, J_2 = 5 Hz, quinolinyl-C_3), 7.53-7.49 (m, 2H, phenyl-C_3, C_5), 3.40 (q, 2H, J_1 = 5, J_2 = 5, J_3 = 10 Hz, propanamide-CH_2), 2.81 (t, 2H, J_1 = 5, J_2 = 5 Hz, propanamide-$COCH_2$); ^{13}C NMR (125 MHz, DMSO-d_6)

δ 172.35 (acetamide-CO), 160.24 (chlorophenyl-C_4), 159.42 (quinolinyl-C_2), 157.27 (phenyl-C_1), 156.75 (chlorophenyl-C_3, C_5), 156.35 (chlorophenyl-C_2, C_6), 155.79 (quinolinyl-C_8), 148.75 (quinolinyl bridge-C_{8a}), 145.44 (quinolinyl-C_7), 144.52 (phenyl-C_2, C_6), 142.72 (quinolinyl-C_3), 134.51 (quinolinyl-C_4), 132.84 (quinolinyl-C_6), 131.85 (quinolinyl bridge-C_{4a}), 129.85 (quinolinyl-C_5), 128.68 (chlorophenyl-C_1), 127.74 (phenyl-C_3, C_5), 126.88 (phenyl-C_4), 52.79 (propanamide-$NHCH_2$), 59.35 (propanamide-CH_2); MS (ESI): *m/z* found 466.46 [M^+]; calculated for $C_{24}H_{20}ClN_3O_3S$ 465.09.

2-((4'-fluoro-[1,1'-biphenyl])-4-sulfonamido)-N-(quinolin-6-yl)propanamide (**42**): Synthesized as per general procedure mentioned in section (4.1.3) using ((4'-fluoro-[1,1'-biphenyl]-4-yl)sulfonyl)glycinoyl chloride (**21**) (1.5 g) and quinolin-6-amine (**29**) (0.66 gm) to get compound **42** as buff white solid, yield 60%; mp 188-190 ºC; FTIR (KBr) cm^{-1}: 3389 (NH-str.), 2867 (Ar-str.), 1674 (C=O-str.), 1134 (SO_2-str.); ^{1}H NMR (500 MHz, DMSO-d_6) δ 10.43 (s, 1H, -NH), 8.83 (s, 1H, quinolinyl-C_2), 8.53 (s, 1H, quinolinyl-C_4), 8.28 (s, 1H, sulfonamide-NH), 7.95-7.92 (m, 3H, fluorophenyl-C_3, C_5, quinolinyl-C_8), 7.85-7.83 (m, 3H, phenyl-C_2, C_6 and quinolinyl-C_7), 7.66-7.62 (m, 3H, fluorophenyl-C_2, C_6 and quinolinyl-C_5), 7.57 (t, 1H, J_1 = 5, J_2 = 10 Hz, quinolinyl-C_3), 7.51 (d, 2H, J = 10 Hz, phenyl-C_3, C_5), 3.82 (q, 2H, J_1 = 5, J_2 = 5, J_3 = 10 Hz, propanamide-CH_2), 2.79 (t, 2H, J_1 = 5, J_2 = 5 Hz, propanamide-$COCH_2$); ^{13}C NMR (125 MHz, DMSO-d_6) δ 164.57 (fluorophenyl-C_4), 163.84 (acetamide-CO), 158.87 (quinolinyl-C_2), 145.87 (phenyl-C_1), 143.15 (quinolinyl bridge-C_{8a}), 141.56 (quinolinyl-C_3), 135.23 (fluorophenyl-C_1, C_3, C_5), 132.42 (phenyl-C_2, C_4, C_6), 130.04 (quinolinyl-C_8), 129.59 (quinolinyl-C_4), 129.30 (quinolinyl bridge-C_{4a}), 128.49 (quinolinyl-C_7), 128.18 (quinolinyl-C_6), 127.65 (quinolinyl-C_5), 126.78 (fluorophenyl-C_2, C_6), 125.84 (phenyl-C_3, C_5), 45.74 (propanamide-CH_2); MS (ESI): *m/z* found 436.64 [M^+]; calculated for $C_{23}H_{18}FN_3O_3S$ 435.11.

3-([1,1'-biphenyl]-4-sulfonamido)-N-(quinolin-6-yl)propanamide (**43**): It was synthesized as per general procedure mentioned in section (4.1.3) using 3-([1,1'-biphenyl]-4-

sulfonamido)propanoyl chloride (**22**) (1.02 g) and quinolin-6-amine (**29**) (0.66 gm) to get compound **43** as yellowish powder, yield 60%; mp 185-187 ºC; FTIR (KBr) cm^{-1}: 3355 (NH-str.), 2874 (Ar-str.), 1703 (C=O-str.), 1147 (SO_2-str.); ^{1}H NMR (500 MHz, DMSO-d_6) δ 10.43 (s, 1H, -NH), 8.86 (s, 1H, quinolinyl-C_2), 8.67 (s, 1H, quinolinyl-C_7), 8.21 (s, 1H, sulfonamide-NH), 7.96-7.85 (m, 6H, biphenyl-C_2, C_3, C_5, C_6, $C_{3'}$, quinolinyl-C_4), 7.75-7.70 (m, 2H, biphenyl-$C_{2'}$, $C_{6'}$), 7.67-7.63 (m, 1H, quinolinyl-C_5), 7.57-7.53 (m, 1H, quinolinyl-C_8), 7.50 (t, 2H, J_1 = 10, J_2 = 5 Hz, biphenyl-$C_{4'}$, $C_{5'}$), 7.43-7.40 (m, 1H, quinolinyl-C_3), 3.20 (q, 2H, J_1 = 5, J_2 = 5, J_3 = 10 Hz, propanamide-CH_2), 2.68 (t, 2H, J_1 = 5, J_2 = 5, propanamide-$COCH_2$); ^{13}C NMR (125 MHz, DMSO-d_6) δ 168.59 (acetamide-CO), 158.90 (quinolinyl-C_2), 156.68 (biphenyl-C_1), 155.67 (quinolinyl-C_6), 146.34 (quinolinyl bridge-C_{8a}), 143.41 (quinolinyl-C_5), 141.76 (quinolinyl-C_3, C_7), 132.68 (quinolinyl-C_8), 130.90 (quinolinyl-C_4), 129.72 (quinolinyl bridge-C_{4a}), 128.72 (biphenyl-$C_{1'}$), 127.54 (biphenyl- C_2, C_6), 125.58 (biphenyl-C_3, C_5), 125.35 (biphenyl-$C_{2'}$, $C_{6'}$), 124.63 (biphenyl-$C_{3'}$), 123.75 (biphenyl-C_4), 123.47 (biphenyl-$C_{4'}$), 122.75 (biphenyl-$C_{5'}$) 50.63 (propanamide-$NHCH_2$), 48.74 (propanamide-CH_2); MS (ESI): *m/z* found 432.62 [M^+]; calculated for $C_{24}H_{21}N_3O_3S$ 431.13.

3-((4'-chloro-[1,1'-biphenyl])-4-sulfonamido)-N-(quinolin-6-yl)propanamide (**44**): Synthesized as per general procedure mentioned in section (4.1.3) using 3-((4'-chloro-[1,1'-biphenyl])-4-sulfonamido)propanoyl chloride (**23**) (1.64 g) and quinolin-6-amine (**29**) (0.66 gm) to get compound **44** as buff white powder, yield 58%; mp 185-186 ºC; FTIR (KBr) cm^{-1}: 3375 (NH-str.), 2882 (Ar-str.), 1682 (C=O-str.), 1158 (SO_2-str.); ^{1}H NMR (500 MHz, DMSO-d_6) δ 10.34 (s, 1H, -NH), 8.82 (d, 2H, J = 5Hz, chlorophenyl-C_3, C_5), 8.70 (s, 1H, quinolinyl-C_2), 8.66 (d, 2H, J = 5Hz, phenyl-C_2, C_6), 8.53 (s, 1H, quinolinyl-C_7), 8.06 (s, 1H, sulfonamide-NH), 7.90 (d, 2H, J = 5Hz, chlorophenyl-C_2, C_6), 7.87-7.83 (m, 1H, quinolinyl-C_3), 7.78-7.73 (m, 2H, quinolinyl-C_4, C_5), 7.61 (t, 1H, J_1 = 10, J_2 = 5 Hz, quinolinyl-C_8), 7.56-7.52 (m, 2H, phenyl-C_3, C_5), 3.45 (q, 2H, J_1 = 5, J_2 = 5, J_3 = 10 Hz, propanamide-CH_2), 2.85 (t, 2H, J_1 = 5,

J_2 = 5, propanamide-$COCH_2$); ^{13}C NMR (125 MHz, DMSO-d_6) δ 172.28 (acetamide-CO), 160.47 (chlorophenyl-C_4), 159.74 (quinolinyl-C_2), 157.48 (phenyl-C_1), 156.25 (chlorophenyl-C_3, C_5), 156.58 (chlorophenyl-C_2, C_6), 155.84 (quinolinyl-C_6), 148.52 (quinolinyl bridge-C_{8a}), 145.85 (quinolinyl-C_7), 144.85 (phenyl-C_2, C_6), 142.28 (quinolinyl-C_3), 134.51 (quinolinyl-C_8), 132.45 (quinolinyl-C_4), 131.48 (quinolinyl bridge-C_{4a}), 129.85 (quinolinyl-C_5), 128.85 (chlorophenyl-C_1), 127.48 (phenyl-C_3, C_5), 126.37 (phenyl-C_4), 52.85 (propanamide-$NHCH_2$), 59.85 (propanamide-CH_2); MS (ESI): *m/z* found 466.28 [M^+]; calculated for $C_{24}H_{20}ClN_3O_3S$ 465.09.

3-([1,1'-biphenyl]-4-sulfonamido)-N-(1H-indol-5-yl)propanamide (**45**): The compound was synthesized as per general procedure mentioned in section (4.1.3) using 3-([1,1'-biphenyl]-4-sulfonamido)propanoyl chloride (**22**) (1.48 g) and 1*H*-indol-5-amine (**30**) (0.60 gm) to get compound **45** as buff white solid, yield 70%; mp 190-192 ºC; FTIR (KBr) cm^{-1}: 3342 (NH-str.), 2865 (Ar-str.), 1689 (C=O-str.), 1138 (SO_2-str.); ^1H NMR (500 MHz, DMSO-d_6) δ 10.24 (s, 1H, -NH), 8.88 (s, 1H, indolyl-C_2), 8.66 (s, 1H, indolyl-C_6), 8.10 (s, 1H, sulfonamide-NH), 7.93-7.82 (m, 6H, biphenyl-C_2, C_3, C_5, C_6, $C_{3'}$, indolyl-C_3), 7.73-7.68 (m, 2H, biphenyl-$C_{2'}$, $C_{6'}$), 7.65-7.61 (m, 2H, indolyl-C_7, -NH), 7.47 (t, 2H, J_1 = 10, J_2 = 5 Hz, biphenyl-$C_{4'}$, $C_{5'}$), 7.42 (s, 1H, indolyl-C_4), 3.24 (q, 2H, J_1 = 5, J_2 = 5, J_3 = 10 Hz, propanamide-CH_2), 2.64 (t, 2H, J_1 = 5, J_2 = 5 Hz, propanamide-$COCH_2$); ^{13}C NMR (125 MHz, DMSO-d_6) δ 168.78 (acetamide-CO), 159.74 (indolyl-C_2), 156.51 (biphenyl-C_1), 155.77 (indolyl-C_5), 146.26 (indolyl bridge-C_{7a}), 143.38 (indolyl-C_3), 141.77 (indolyl-C_6), 132.78 (indolyl-C_4), 130.68 (indolyl-C_7), 129.35 (indolyl bridge-C_{4a}), 128.57 (biphenyl-$C_{1'}$), 127.24 (biphenyl- C_2, C_6), 125.55 (biphenyl-C_3, C_5), 125.27 (biphenyl-$C_{2'}$, $C_{6'}$), 124.64 (biphenyl-$C_{3'}$), 123.77 (biphenyl-C_4), 123.38 (biphenyl-$C_{4'}$), 122.71 (biphenyl-$C_{5'}$) 50.78 (propanamide-$NHCH_2$), 48.55 (propanamide-CH_2); MS (ESI): *m/z* found 420.43 [M^+]; calculated for $C_{23}H_{21}N_3O_3S$ 419.13.

3-((4'-chloro-[1,1'-biphenyl])-4-sulfonamido)-N-(1H-indol-5-yl)propanamide (**46**): Synthesized as per general procedure mentioned in section (4.1.3) using 3-((4'-chloro-[1,1'-biphenyl])-4-sulfonamido)propanoyl chloride (**23**) (1.64 g) and 1*H*-indol-5-amine (**30**) (0.60 gm) to get compound **46** as buff white solid, yield 72 %; mp 189-191ºC; FTIR (KBr) cm^{-1}: 3378 (NH-str.), 2873 (Ar-str.), 1687 (C=O-str.), 1214 (SO_2-str.); ^{1}H NMR (500 MHz, DMSO-d_6) δ 10.27 (s, 1H, -NH), 8.79 (d, 2H, *J* = 5Hz, chlorophenyl-C_3, C_5), 8.72 (s, 1H, indolyl-C_2), 8.64 (d, 2H, *J* = 5Hz, phenyl-C_2, C_6), 8.55 (s, 1H, indolyl-C_6), 8.13 (s, 1H, sulfonamide-NH), 7.87 (d, 2H, *J* = 5Hz, chlorophenyl-C_2, C_6), 7.88-7.84 (m, 1H, indolyl-C_3), 7.76-7.71 (m, 2H, indolyl-C_7, -NH), 7.57-7.53 (m, 2H, phenyl-C_3, C_5), 7.42 (s, 1H, indolyl-C_4), 3.47 (q, 2H, J_1 = 5, J_2 = 5, J_3 = 10 Hz, propanamide-CH_2), 2.84 (t, 2H, J_1 = 5, J_2 = 5, propanamide-$COCH_2$); ^{13}C NMR (125 MHz, DMSO-d_6) δ 172.37 (acetamide-CO), 160.52 (chlorophenyl-C_4), 159.89 (indolyl-C_2), 157.51 (phenyl-C_1), 156.28 (chlorophenyl-C_3, C_5), 156.60 (chlorophenyl-C_2, C_6), 155.88 (indolyl-C_5), 148.63 (indolyl bridge-C_{7a}), 145.50 (indolyl-C_3), 144.88 (phenyl-C_2, C_6), 142.30 (indolyl-C_6), 134.48 (indolyl-C_4), 132.43 (indolyl-C_7), 131.37 (indolyl bridge-C_{4a}), 129.59 (chlorophenyl-C_1), 128.52 (phenyl-C_3, C_5), 127.54 (phenyl-C_4), 59.58 (propanamide-$NHCH_2$), 52.83 (propanamide-CH_2); MS (ESI): *m/z* found 454.61 [M^+]; calculated for $C_{23}H_{20}ClN_3O_3S$ 453.09.

4.2.6 Biology

4.2.6.1 *In-vitro* AChE and BChE inhibition assays:

AChE and BChE inhibition assays were performed according to the earlier reported protocol with minor modifications[79]. AChE from Electrophorus electricus (electric eel) (CAS No. 9000-81-1) and BChE from equine serum (Equus caballus) (CAS No. 9001-08-5) were procured from Sigma Aldrich. Acetylthiocholine iodide (ATCI), Butyrylthiocholine iodide (BTCI) and 5,5′-dithiobis (2-nitrobenzoic acid) (DTNB-Ellman's reagent) were obtained from Himedia. The assays were performed in phosphate buffer (pH 7.4). DNP was used as the

standard compound for the enzyme inhibition assays. The percentage inhibition of the compounds was calculated at higher doses (100 and 50 µM) to obtain a valid concentration range for the IC_{50} assay. Six different concentrations of 500 µM, 200 µM, 100 µM, 50 µM, 25 µM, and 1 µM of test compounds were used to determine the IC_{50}. 50 µL of AChE or BChE and 20 µL of test or standard compounds were incubated in the 96 well plate for 30 min. at rt. 100 µL of DTNB was added to the above solutions. The substrate *i.e.* ATCI or BTCI was then added and absorbance recorded after 30 min. of incubation at 415 nm using Synergy HTX multi-mode reader (BioTek, USA). The IC_{50} values were calculated using absorbance obtained from the test and standard compounds. The assays were performed in triplicate and in three independent runs.

4.2.6.2 *In-vitro* MMP-2 inhibition assay

MMP-2 inhibitor screening assay kit (Fluorometric) was purchased from Abcam (ab139447). Seven different concentrations (1000-0.1 nM) of the test compounds were used in the enzyme inhibition studies. MMP-2 enzyme (Human, Recombinant) (20 µL) was added to each well of the plate in the final concentration of 1.16 U. The test compounds in seven different concentrations (20 µL) were added to the enzyme followed by the incubation of the plate for 60 min. to allow for enzyme-test compound interaction. The fluorogenic substrate in the final concentration of 4 µM (10 µL) was added to the incubated mixture and the volume was made up to 100 µL with fluorogenic assay buffer. Ex/Em: 328/420 was used to record the fluorescence spectra in a microplate reader (HTX multi-mode reader, BioTek, USA) at 1 min interval for 10 min. The assay was performed in triplicate with calibration sample containing 10 µL (4 µM) of the substrate and 90 µL of assay buffer, control without inhibitor and inhibitor containing 20 µL (6.5 µM) of N-Isobutyl-N-(4-methoxyphenylsulfonyl) glycyl hydroxamic acid (NNGH). The activity was expressed in relative fluorescent units (RFU) and the control

reaction was used to calculate the percentage inhibition. The data was processed by using GraphPad Prism 5, Excel and IC_{50} were calculated by using the formula- $Vi/Vo = 1/1+([I]/IC_{50})$

Where *Vi* is initial velocity of product formation in the presence of inhibitor Vo and I is the initial velocity in the absence of inhibitor I.

4.2.6.3 AChE enzyme Kinetics

Enzyme kinetic study was performed to understand the mechanism of enzyme action of compound **41**. Seven different substrate concentration used in the kinetic study was in the range of 20-70 nM. Compound **41** was used in three different concentration ranges of 1180 to 440 nM respectively. Each concentration of compound **41** was used at seven different concentrations of the substrate. The activity was measured for 10 min at an interval of 2 min in the absence and presence of compound **41** at 415 nm using Synergy HTX multi-mode reader (BioTek, USA). Product formed during the time frame of 10 min was calculated by Beer-Lambert law. The velocity of the enzyme reaction was obtained from plotting the product formed during 10 min. Vmax, Km were calculated by Michaelis-Menten nonlinear regression graph and Lineweaver-Burk reciprocal linear regression plots were used to determine the mechanism of enzyme inhibition by GraphPad Prism 5.2.

4.2.6.4 *In-vitro* metal chelation assay

Compound **41** (500 µM) was dissolved in 3 mL of deionized water and pH was monitored. The solution obtained was scanned under UV spectroscopy in the range of 200-760 nM. 1.3 mg of $FeCl_3.6H_2O$ was dissolved in 3 mL of water to get 500 µM colorless solution. The solutions of compounds and $FeCl_3.6H_2O$ were mixed, pH was monitored and were scanned under UV in Shimadzu UV-Vis Spectrophotometer. The spectra were plotted on excel comparing the UV shift before and after complexation. Finally, the pH of the solution was raised to 7.4 by adding an additional amount of DIPEA to the same solution followed by UV scanning. Metal chelation assay was performed in triplicate.

4.2.6.5 Inhibition assay of metal induced $A\beta_{1-42}$ aggregation

Aβ-redox active metal produces ROS causing neuronal cell death. Metal ions along with AChE were found to induce the Aβ aggregation[82]. Thioflavin T (ThT) assay was performed to determine the inhibition potential of compound 41 against Fe^{+3} induced $A\beta_{1-42}$ aggregation[83]. $A\beta_{1-42}$ (Sigma) was dissolved in phosphate buffer (PBS, 10 mM, pH 7.5), compound 41 was dissolved in DMSO and diluted with PBS. Different proportions of the $A\beta_{1-42}$: Inhibitor (1:0.5, 1:1, 1:2) were used in the ThT assay. The final concentration of $A\beta_{1-42}$ compounds 41 and Fe^{+3} was 10 μM (2μL), 0.5, 10, 20 μM (2μL) and 10 μM (16 μL) respectively. The mixtures were incubated at room temperature for 48h in dark. The fluorescence intensities of the incubated mixtures were measured at the end of experiment by adding 178 μL of 20 μM ThT at excitation and emission wavelengths of 485 and 528 nm respectively in Synergy HTX multi-mode reader.

4.2.6.6 Confocal Fluorescence Imaging

The assay mentioned in section 4.2.5 was further used for the confocal fluorescence imaging. Fluorescence dye ThT; $A\beta_{1-42}$ and ThT; $A\beta_{1-42}$; $A\beta_{1-42}$ and $FeCl_3$; $A\beta_{1-42}$, $FeCl_3$ and ThT; $A\beta_{1-42}$, $FeCl_3$, compound 41 and ThT; compound 41 and ThT; compound 41 alone were incubated and mounted on the glass slide using DABCO (Sigma, CAS-280-57-9) as fixing agent. The images were taken at 40X using FITC fluorescence cube at 494 nm excitation and 518 nm emissions. The ZEISS LSM 700 laser scanning confocal microscope was used for imaging. Experiments containing 20 mM of compound 41 was used for confocal imaging[84].

4.2.6.7 Cytotoxicity assay

The synthesized compounds were screened for cytotoxicity against kidney epithelial cells (VERO) by MTT assay. The cells were harvested and 10^5 cells were plated into each well in 100 μL of Eagle's minimum essential medium (EMEM). The well plates were incubated for 24 hours. The test compounds were freshly prepared at five different concentrations ranging from 1 to 80 μM and were added to the wells containing the seeded cells. The cells containing

compounds were incubated for 72 hours. The incubation was followed by the addition of 0.5% solution of 3-(4,5-dimethyl-2-thiazolyl)-2,5-diphenyl-tetrazolium bromide (MTT) in phosphate buffered saline at 20 µL/well and incubation for another 4 hours. Then, 1 mL of DMSO was added as a solubilizing agent and the percentage of viable cells was determined by measuring the absorbance at 570 nm using Synergy HTX multi-mode reader. The measured absorbance was normalized with the negative control[85].

4.2.6.8 MC65 cell line assay

MC65 cell line was obtained as a kind gift from Dr. George M. Martin of the University of Washington[86]. The MTT assay kit was purchased from Himedia. MC65 cells were grown in MEM, washed with PBS and were resuspended in MEM. Further, 5×10^4cells/well were plated in the 96 well plates. The cells were incubated with +TC (Tetracycline) and –TC in CO_2 incubator (Heal force, Germany). In the test group TC was absent (TC-). Test compound 41 (1-70µM) was added and cells were incubated at 37ºC for 12 h. At the end of 12 h, (3-(4,5-Dimethylthiazol-2-yl)-2,5-diphenyltetrazolium bromide (MTT) was added (20 µL, 5 mg/mL) and the cells were incubated for another 4 h. The medium was removed and the formazan crystals produced were dissolved in 150 µL of dissolving solvent (DMSO: H2O, 1:1). The absorbance was immediately recorded at 570 nm using Synergy HTX multi-mode reader and the response was expressed in percentage cell viability relative to +TC as a control. The assay was performed in triplicate and in three independent runs [79].

4.2.6.9 Antioxidant Activity (DPPH assay)

The DPPH radical-scavenging effect was measured according to the previously reported protocol[79]. Briefly, 100 µL of drug solutions of concentration ranges 20µM, 40 µM, 80µM and 160 µM were added to 96-well plate followed by addition of 100 µL (200 µM) solution of DPPH. Control wells received 20, 100 and 100µL of DMSO, buffer and DPPH solution respectively. The plate was shaken vigorously at 30 °C for 25 min in the dark. The changes in

absorbance of all the samples and standard (ascorbic acid) were measured at 517 nm. The absorbances obtained were used to calculate the EC_{50}. The assays were performed in triplicate and in three independent runs. Ascorbic acid was used as the standard for the DPPH assay[87].

4.2.6.10 $A\beta_{1-42}$ induced ICV Rat Model of AD

Adult male Wistar rats (200-250 g) were used for the study. The animals were divided in to seven groups: (i) control, (ii) vehicle, (iii) $A\beta_{1-42}$ (iv) DNP (v) compound 41 (0.5 mg/kg) (vi) Compound 41 (1 mg/kg) (vii) compound 41 (2 mg/kg) containing six animals each. The animals were anesthetized with ketamine (100 mg/kg, i.p) and xylazine (30 mg/kg, i.p) and fixed on stereotaxic apparatus (Stoelting, USA) for surgery. All the groups (except the surgery control *i.e.* vehicle, received equal volume of normal saline and control group) were injected with 4 µL of $A\beta_{1-42}$ (2 µM/µL in normal saline) unilaterally at the coordinates: -4.0 mm anteroposterior, -2.5 mm mediolateral, and -3.5 mm dorsoventral from Bregma. The animals were kept for six days to get recovery from surgery. Compound 41 was dissolved in 0.1% of CMC and administered i.p, once a day at three different doses (0.5, 1 and 2 mg/kg) for fifteen consecutive days[88]. Approval from animal ethical committee was granted (Protocol No. Dean/13-14/CAEC/342) and surgical processes were carried out under aseptic conditions.

4.2.6.11 Y-Maze Test

The test was performed to evaluate the immediate working memory. The experimental design and doses used in the study are already mentioned in section 4.2.7. The test was carried out during last five days of treatment period. Training session of 15 min. was carried out after dosing in which animals were placed in Y-maze with the novel arm closed. After four-hour training sessions, the main study was performed. In this period the animal was kept at the center of arm to explore all the three arms. The experiment was performed for 15 min. and entry of the rats into each of the arms was recorded within camera and repeated arm entry was considered as the sign of memory impairment. Further, consecutive arm choices (ABC, BCA,

CAB not BAB) and novel arm entry were considered as the memory improvement. The memory improvement score was calculated using the equation:

% alternation = (number of alternations/ (total arm entries) – 2) X 100.

4.2.6.12 Pharmacokinetic Studies

Male Wistar rats of 200-250g (n=3) were used for pharmacokinetic studies. Compound 41 was suspended in 0.1% CMC and administered by i.p route at dose of 50 mg/kg. After administration, the animals were anesthetized with ether and blood, CSF and brain samples were collected at five time point (0.5, 1, 2, 4 and 6 hr). 250 µL of blood was collected for plasma related experiments by cardiac puncture in heparin containing tubes. Blood samples were centrifuged at 3500 rpm for 10 min (4 °C) to isolate plasma. 25 µL of plasma and 100 µL of mobile phase (methanol: acetonitrile, 0.5:0.5) were mixed and vortexed for one min followed by centrifugation at 12300 rpm for 5 min. 20 µL aliquot of the resulting solution was injected into the HPLC (Agilent 1260 infinity II Quaternary LC). 25 µL of CSF was collected followed by dilution with 50 µL of mobile phase and vortex for one min. 20 µL of the filtered CSF mixture was injected in HPLC for analysis. Accumulation of the drug within the hippocampus was determined by isolating brains from the animals subsequent to collecting blood and CSF. Animals were sacrificed by cervical dislocation, following which their brain was isolated, rinsed by cold saline and stored at -80 °C for further use. On the day of assay frozen tissues were thawed at room temperature and hippocampus was isolated. Hippocampal tissues were homogenized with 0.5 mL of methanol for 1 min followed by vortexing for 1 min. 25 µL aliquot was transferred into an Eppendorf tube. To each sample, 25 µL of methanol was added, and the samples were centrifuged at 11 000 g for 5 min. A 20 µL aliquot of the supernatants was diluted to 60 µL with the mobile phase and a 20 µL aliquot was injected into HPLC. Quantification of the drug concentration in each aliquot was achieved by using the

standard curve method. Half-life was calculated using the GraphPad software, fitting to a single-phase exponential decay equation.

4.2.7 In silico studies

4.2.7.1 Molecular docking

The docking study was performed for two enzymes: AChE and MMP-2. The crystal structures 4EY7, 1HOV and 1IYT of AChE, MMP-2 and $A\beta_{1-42}$ respectively, were obtained from RCSB (http://www.rcsb.org). The molecular docking was performed using autodock-4.2.1 program. Autogrid-4 was used to generate grid maps for both the enzyme with atom type A, C, HD, NA, N, OA, S, Br, Cl, I, and F. The grid box of dimension 78X90X102 with grid center 9.639, -53.563, -25.052; 66X64X62 with grid center 9.501, 16.835, 17.941 and 114X66X126 with grid center -0.616, -0.065, 1.269 for 4EY7, 1HOV and 1IYT respectively for grid map calculations. The ligands and water molecules present in the protein were removed, polar hydrogens were added and Kollman charge were assigned. Docking was done using Lamarckian genetic algorithm with 27,000 generations and 100 docking runs. The conformation with the lowest binding energy was further analyzed for interaction using DS-visualizer 2016. [89]

4.2.7.2 Field-based QSAR

The field-based QSAR models for AChE and MMP-2 were developed using the training set of 12 of the 16 compounds with the grid spacing of 1 Å and PLS factors of 2. The training set was selected using randomization. Various models were generated using extended Gaussian field with Gaussian steric, electrostatic, hydrophobic, hydrogen bond donor, hydrogen bond acceptor, and aromatic ring fields. The best model was selected using numerous statistical parameters and 3D contour maps were developed using QSAR visualization modules [90].

4.3 Results & discussions

4.3.1 Rational of drug design and discovery

The new compounds were created using a hybrid of database mining techniques and pharmacophore methods. Donepezil along with few of the MMP-2 inhibitors as well as pharmacophoric features from Ion chelators were selected to develop the prototypical pharmacophores (as visualized in Figure 4.1). Following the development, the "Zinc15" and "Asinex" databases' databases were mined using the developed pharmacophores. The obtained compounds of comparable pharmacophoric features were then put through a variety of filters, including toxicity, *in-silico* BBB permeability, and drug-likeness characteristics. The chosen compounds were docked to find functional groups and fragments that would be crucial for interacting with the targets (AChE and MMP-2).

Druglikeness is a qualitative paradigm that is essential to drug design. It measures how much a substance possesses properties that are favourable to pharmacological efficacy, primarily focusing on elements that affect bioavailability. The molecular structure is used to evaluate this idea in advance of synthesis and experimental confirmation. A molecule possessing characteristics necessary for overcoming biological barriers and reaching therapeutic efficacy, is said to be drug-like. These properties include solubility in both aqueous and lipophilic environments, since, an orally administered drug necessitates passage through the intestinal lining, circulation in aqueous blood, and penetration of lipid-based cell membranes to access intracellular compartments.

Lipophilic cellular membrane characteristics are primarily determined by 1-octanol, a medium-chain fatty alcohol. The logarithm of the octanol-water partition coefficient, denoted as LogP, is a predictive measure for the solubility of potential oral drugs. This coefficient, known as "cLogP," can be predicted computationally to assess a compound's likelihood for oral administration. Potency at the biological target is a crucial criterion in drug design, with high potency reducing the risk of non-specific, off-target pharmacology and allowing for lower total doses. Ligand efficiency and lipophilic efficiency also play a role in evaluating drug candidates.

Molecular weight, a critical determinant for drug-likeness, is a critical factor, with smaller molecules being more favourable due to their enhanced diffusion characteristics. Most marketed drugs have molecular weights between 200 and 600 Daltons, with a majority falling below 500 Daltons, highlighting the importance of molecular weight in optimizing drug properties for therapeutic applications.

As with any drug design, the trade-off between maximizing binding to the target enzyme and reducing toxicity or off-target effects must be carefully considered. Compound synthesis and optimization are frequently guided by medicinal chemistry techniques, such as computer modeling and structure-activity relationship (SAR) studies. The activity of compounds targeting acetylcholinesterase in the present series is influenced by the presence of electron-withdrawing or electron-donating substituents on the quinoline ring. The size and shape of substituents play a critical role in binding to the enzyme, while the hydrophobicity or hydrophilicity of substituents significantly impacts solubility and absorption, essential factors for effective drug delivery. Hence, these factors were given close consideration while finalising the series to be synthesized.

Moreover, factors other than the electron-withdrawing groups demonstrate an enhanced interaction with the target enzyme, such as steric properties, including the size and shape of substituents, which could affect the binding of the compound to acetylcholinesterase. The bulkiness of certain substituents can also influence the molecule's ability to fit into the enzyme's active site. Additionally, the strategic placement of functional groups was identified as a means to enhance interactions with the target enzyme, and conformational flexibility emerges as a crucial factor for optimal binding to the active site of acetylcholinesterase. These considerations collectively influenced the design of targeted compounds.

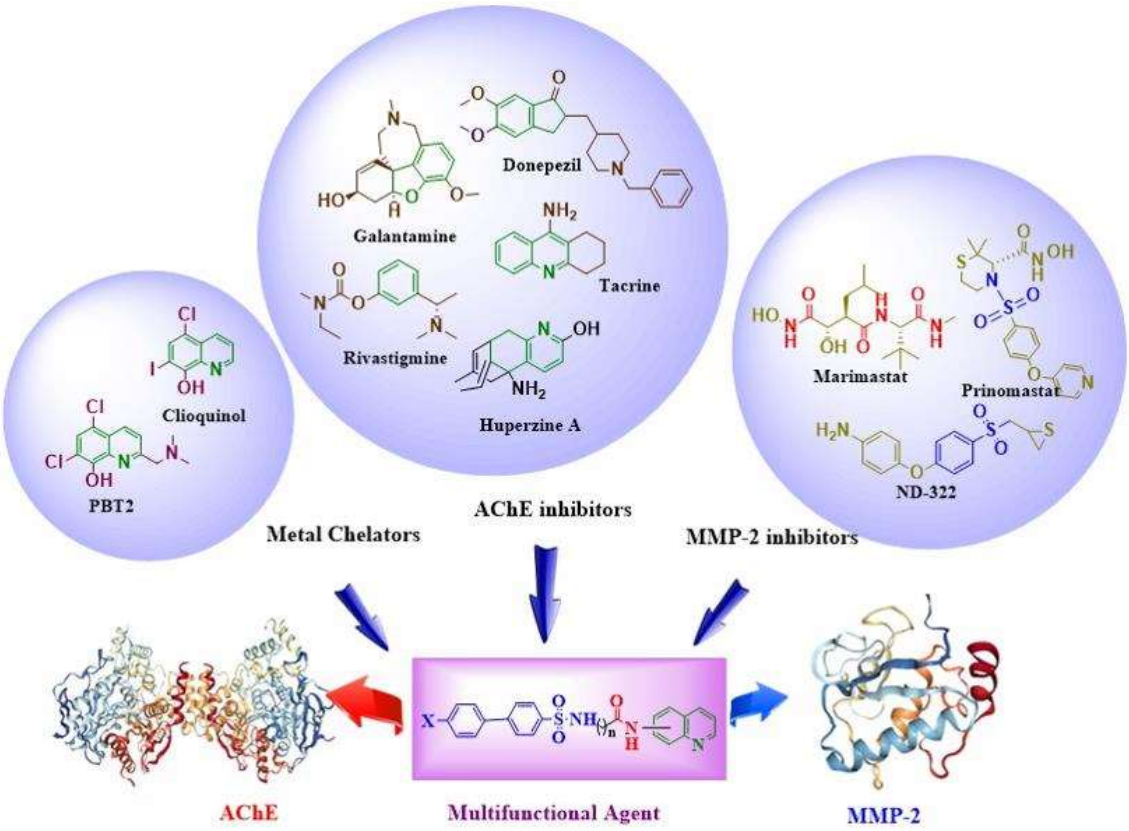

Figure 4.1 Design strategy for the multitargeted compounds

4.3.2 Chemistry

Compounds 10 to 17 were prepared by reacting substituted aromatic sulfonyl chlorides with two or three carbon length amino acids as linkers. First step of the synthesis protocol was carried out in a mixture of water and acetone with sodium bicarbonate acting as the base. The compounds were characterized by FT-IR, ^{1}H, ^{13}C NMR spectroscopy and Mass spectrometry. The acidic groups in the compounds were further converted to acid chlorides using thionyl chloride. The acid chlorides (i.e., compounds 18 to 26) thus obtained, were found to be highly reactive and hence were immediately used for the next step. Final products, 31 to 46, were obtained by reacting acid chlorides (18-26) with different aminoquinolines or aminoindoles (Scheme 1).

4.3.3 Biological Evaluation

4.3.3.1 *In-vitro* AChE, BChE and MMP-2 enzyme inhibition assays

The MMP-2 inhibition activity of the compounds was in the range of 18.24±1.61 to 108.16±0.58nm, while the AChE inhibition was in 2.06±0.27 μM to 352.6±0.18 μM range. Due to varying structural features. The results of the inhibition studies followed the pattern observed in the *in-silico* study.

Compound 31, synthesized and screened for the MMP-2, AChE and BChE enzyme assays, displayed moderate activity against MMP-2 (IC_{50}108.16±0.58 nM), AChE (IC_{50} 68.27±0.76 μM) and BChE (IC_{50} >100 μM) where, an increase in the potency was observed by incorporating various substitutions in the other compounds of the series.

The substitution of a phenyl hydrogen with fluoro group did not yield significant change in the IC_{50} (compound 32, MMP-2 IC_{50} 103.41±0.85 nM, AChE IC_{50} 60.28±0.68 μM). However, substitution of the same with chloro group yielded significant improvement in inhibition as seen in compound 33 (MMP-2 IC_{50} 78.05±0.530 nM, AChE IC_{50} 16.37±0.52 μM) with the increased linker length by a single carbon atom.

The S1 and S2 subsites of MMP-2 were found to interact with the π cloud of the aromatic groups leading to an approximately 50 % decrease in its IC_{50} (MMP-2 IC_{50} 54.15±0.85 nM, AChE IC_{50} 52.54±0.54 μM).

Different substitution positions of aminoquinolines were explored to understand the SAR of the molecules. 8-quinolinyl series (37-41) showed increased potency when compared with 3-quinolinyl series (31-36). Further, *p*-methoxy compounds 37 and 38 displayed considerable increase in potency (compound 37, MMP-2 IC_{50} 33.58±0.88 nM, AChE IC_{50} 50.87±1.28 μM and compound 38 MMP-2 IC_{50} 22.85±0.28 nM, AChE IC_{50} 45.50±0.96 μM). The biphenyl 8-quinolinyl series (39-41) also followed the trend of biphenyl 3-quinolinyl series and *p*-chloro

group containing biphenyl compound 41 was found to be most effective for MMP-2 inhibition and very effective for AChE inhibition (MMP-2 IC_{50} 18.24 ±1.62 nM, AChE IC_{50} 4.28±0.15 μM, BChE IC_{50} 1.32±0.02 μM).

As mentioned earlier, the electron withdrawing groups are seem to be important for activity but fine-tuning between the electronegativity and size of group is also essential. Compound 42 possessed inhibition potential similar to that of the compound 41 (MMP-2 IC_{50} 19.18 ±0.19 nM, AChE IC_{50} 3.58±0.87 μM, BChE IC_{50} 9.95±0.10 μM). The designed molecules were selective for AChE, when compared to BChE. Compounds 31-33, mono-phenyl 3-quinolinyl series were found to be inactive with BChE, while, compounds 39-44 (Bi-phenyl 8-quinolinyl series) showed moderate activity against BChE. Further, compound 41 emerged as the most potent compound of the series with an IC_{50} of 01.32±0.02 μM, which was comparable with Donepezil (IC_{50} 1.20±0.03 μM) for BChE inhibition. Indole containing compounds 45 and 46 also produced good inhibition but had weak interactions with $A\beta_{1\text{-}42}$ protein in *in-silico* studies (**Table 4.1**).

Table 4.1 Structures and enzyme inhibition activities of the synthesized novel 3-((4-substituted) sulfonamido)-N-(indole/quinolin-3/6/8-yl)ethan/ propanamides.

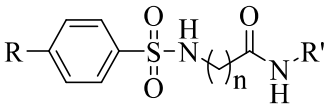

ID.	R	R'	n	IC_{50} (nM) of MMP-2	IC_{50}(µM) of AChE	IC_{50}(µM) of BChE	[a]S.I
31	H	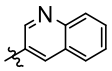	1	108.16±0.58	68.27±0.75	>100	-----
32	F	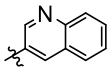	1	103.41±0.84	60.28±0.68	>100	-----
33	Cl	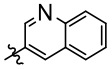	2	78.05±0.53	16.37±0.52	>100	-----
34	FPh	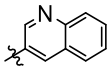	1	54.15±0.85	52.54±0.54	49.62±0.25	1.05
35	Ph	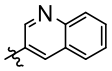	2	66.62 ±1.08	48.68±0.09	82.83±0.18	0.58
36	ClPh	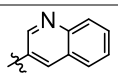	2	38.24 ±0.27	24.68±0.09	39.28±0.05	0.63
37	OMe		1	33.58±0.88	50.87±1.28	>100	-----
38	OMe		2	22.85±0.28	45.50±0.96	>100	-----
39	FPh		1	37.58±1.25	40.80±1.02	10.74±0.08	3.80
40	Ph		2	61.83 ±0.20	352.6±0.18	15.74±0.04	22.40
41	ClPh		2	18.24 ±1.61	4.28±0.14	01.32±0.02	3.24
42	FPh	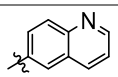	2	19.18 ±0.19	3.58±0.87	09.95±0.10	0.36
43	Ph	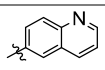	2	62.52 ±0.21	24.35±4.02	20.28±0.25	1.20

44	ClPh	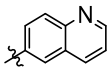	2	34.96 ±0.40	6.247±4.55	07.85±0.05	0.80
45	Ph	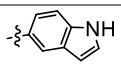	2	22.57 ±0.45	2.064±0.27	>100	-----
46	ClPh	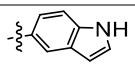	2	85.28 ±0.86	28.84±0.51	>100	-----
NNGH	-----	-----	-	14.21±0.42	-----	-----	-----
DNP	-----	-----	-	>1000	0.023±0.018	1.28±0.03	

[a] S.I. (Selectivity Index) = (IC_{50} AChE/IC_{50} BChE); N-Isobutyl-N-(4-methoxyphenylsulfonyl)glycyl hydroxamic acid (NNGH); Donepezil (DNP).

4.3.3.2 AChE enzyme kinetics

The mechanism of action and binding pattern of compound 41, with the enzyme, was determined by enzyme kinetic studies. Graphical analysis of the reciprocal Lineweaver-Burk plots showed an increase in both slopes (decreased Vmax) and intercepts (higher Km) with increasing inhibitor concentrations. The enzyme kinetic pattern established a non-competitive inhibition pattern against AChE (**Figure .4.2**).

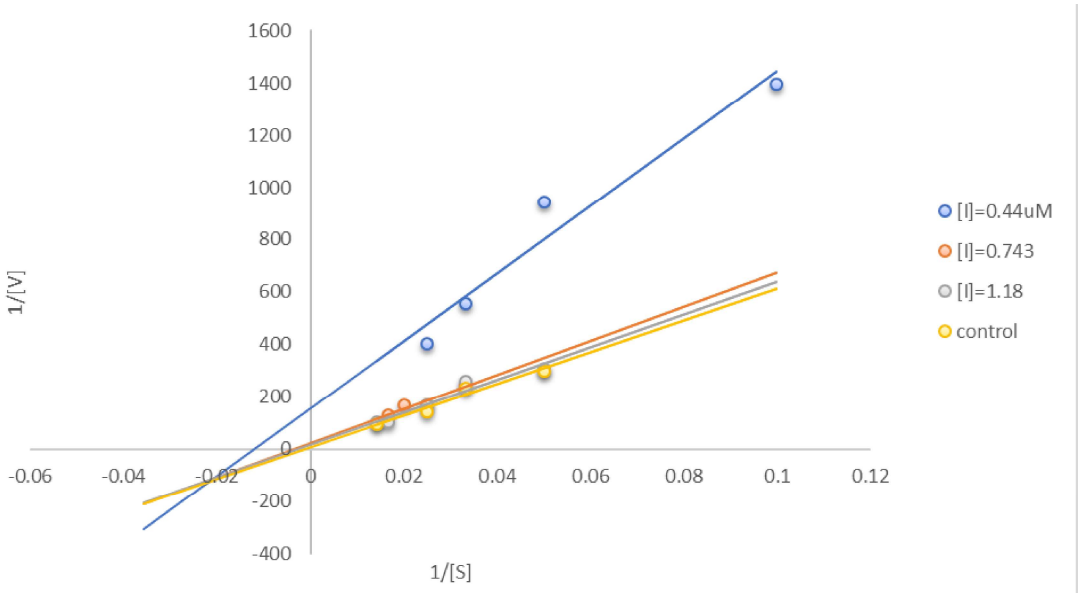

Figure 4.2 Lineweaver-burk plot; Enzyme kinetics showing non-competitive pattern of binding of compound 41 with AChE.

4.3.3.3 Metal chelation assay

Biometals (Cu, Fe, and Zn) are found to be actively involved in the Aβ aggregation. The harmful oligomers of Aβ are stabilized by Aβ-metal complexation in most of the cases [91]. Cu^{2+} and Fe^{2+} were reported to be involved in ROS production leading to neuronal death [92]. The prepared compounds were explored for their metal chelation property by using $FeCl_3.6H_2O$. Compound 41 showed metal chelating property as witnessed by their UV and FTIR spectra. UV spectra of the metal complexes showed a significant shift from the parent compound (**Figure 4.3**) [93, 94].

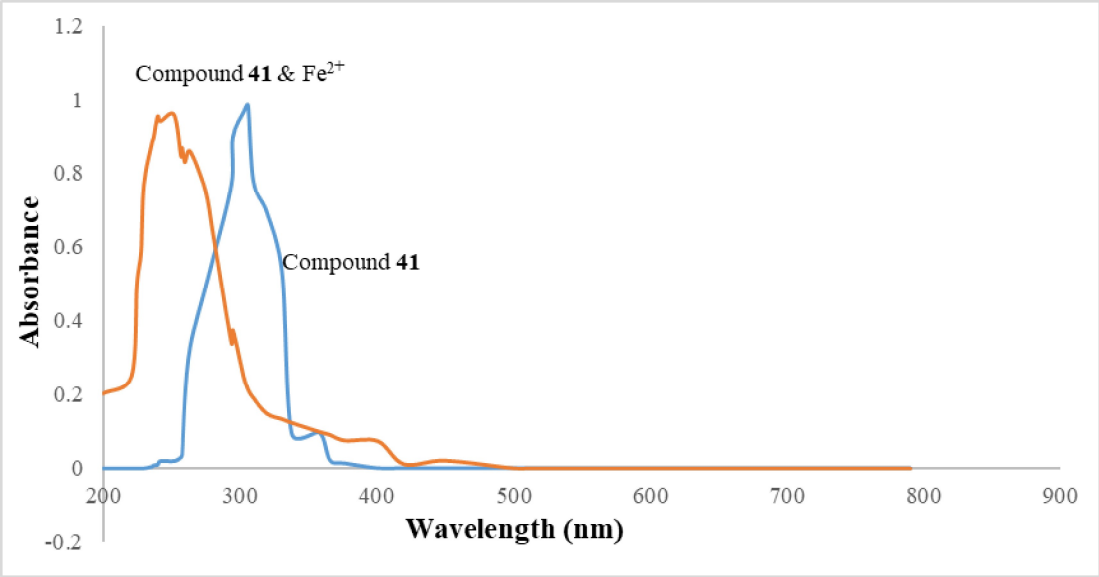

Figure 4.3 UV- spectra of the compound 41 showing shift in λ_{max} of metal chelate

4.3.3.4 Inhibition assay of metal induced $A\beta_{1-42}$ aggregation and confocal fluorescence imaging

The designed compounds showed excellent metal chelation property, therefore metal induced aggregation of $A\beta_{1-42}$ assay was performed to determine the potency of the lead compound 41. $A\beta_{1-42}$ upon incubation with the metal showed 100% aggregation. DNP, at a dose of 20 μM produced significant inhibition of metal induced $A\beta_{1-42}$ aggregation and Compound 41 was found to be more effective than DNP. It inhibited more than 50% of $A\beta_{1-42}$ aggregation when

compared with Fe^{+3}+ $A\beta_{1-42}$ and $A\beta_{1-42}$ groups (Figure 4.4A). Confocal imaging was performed to comprehend the interaction of $A\beta_{1-42}$, $FeCl_3$ and compound 41 at molecular level. Fluorescent background was obtained when dye ThT was used (Figure 4.4B). $A\beta_{1-42}$ aggregate was obtained when it was incubated and treated with ThT (Figure 4C) whereas, the fluorescence disappeared when $A\beta_{1-42}$ alone and $A\beta_{1-42}$ was incubated with the metal devoid of ThT. These blank images ascertained that neither $A\beta_{1-42}$ and metal nor their combinations showed any background noises in the absence of ThT. $A\beta_{1-42}$ incubated with metal showed aggressive plaque deposition (Figure 4D) while the plaques were disaggregated on treatment with compound 41 (Figure 4.4E).

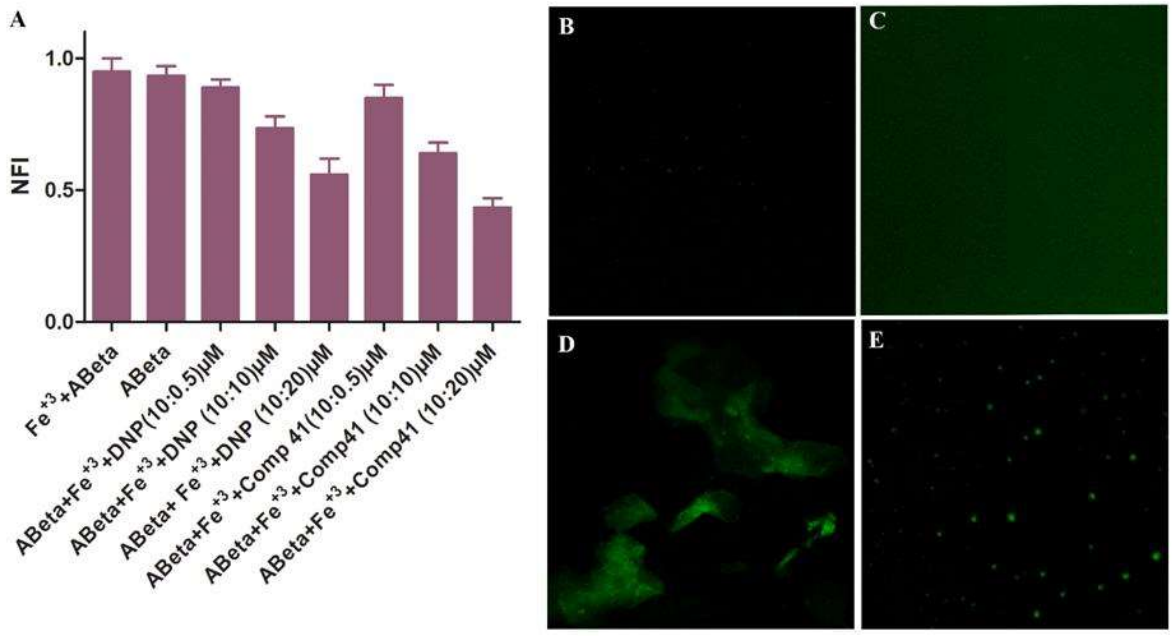

Figure 4.4 Inhibition assay of metal induced Aβ1-42 aggregation and its confocal imaging: (A) metal induced $A\beta_{1-42}$ aggregation assay (One-way ANOVA followed by one-way analysis of variance*** $p < 0.0001$), error bars represent the standard deviation (SD)

4.3.3.5 Cytotoxicity assay

Cytotoxicity of the most active species, compound 41 was determined on VERO cell line by 3-(4,5- dimethylthiazol-2-yl)-2,5-diphenyltetrazolium bromide (MTT) assay. Cells were

exposed to five different concentrations of compound 41 (1, 10, 20, 40 and 80µM) and no significant changes were observed with respect to the cell viability of the control as well as the treated cells even at a high dose of 80 µM (Figure 4.5).

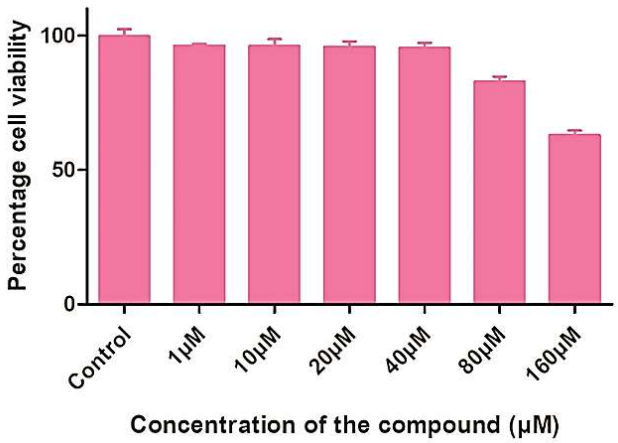

Figure 4.5 Cytotoxicity assay of compound 41 on VERO cell lines

4.3.3.6 Neuroprotection assay using MC65 cell line

Neuronal death has been found to be associated with AD, and ROS are considered to be mainly responsible, among other factors. The mutated neuronal cell line MC65 itself produces Aβ in the absence of tetracycline (TC-) leading to the generation of ROS. Compound 41 showed significant decrease in Aβ production when compared with TC- cells at doses of 50 and 100 µM (Figure 4.6).

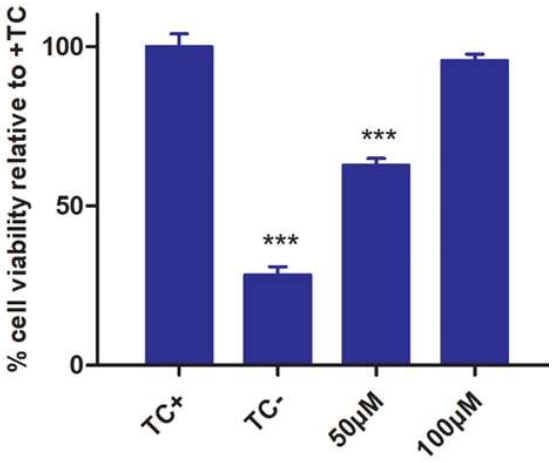

Figure 4.6 Neuroprotection assay of compound 41 (50 and 100 µM) on MC 65 cell line (One-way ANOVA followed by Newman-Keuls multiple comparison test comparison all pair of column *** $p < 0.0001$).

4.3.3.7 Antioxidant activity evaluation

This method measures the hydrogen atom/ electron donating capacity, and is based on the reduction of DPPH (1, 1-Diphenyl-2-picrylhydrazyl), a stable free radical of purple color, to the yellow colored 1, 1-diphenyl-2-picryl hydrazine. Indole containing compounds 45 and 46 were found to be less active than their quinoline counterparts (31-44). Biphenyl quinoline containing compounds showed better free radical scavenging property than their monophenyl analogues. In DPPH assay, it was found that quinoline nucleus is mainly responsible for the antioxidant activity (Table 4.2).

Table 4.2 DPPH assay of the synthesized compounds.

Comp.	EC_{50} (µM)DPPH assay
31	10.85±1.54
32	9.52±0.97
33	11.88±1.24
34	8.24±0.88
35	6.89±1.07

36	9.03±0.85
37	12.54±1.20
38	10.54±1.00
39	7.54±1.22
40	8.55±0.95
41	9.45±0.77
42	9.40±1.37
43	7.26±0.98
45	18.84±1.41
46	17.55±1.78
Ascorbic acid	3.47±0.34

4.3.3.8 Behavioral Studies

The $A\beta_{1-42}$ was injected (icv) to the hippocampal region of the brains of adult male Wistar rats. $A\beta_{1-42}$ induced rats were treated once a day with three different doses (0.5 mg/kg, 1 mg/kg and 2mg/kg) of the most potent compound **41**. Y-maze test was used to study the hippocampal-dependent spatial working memory of animals and was assessed based on the spontaneous alteration score. Y-maze test was performed for 5 consecutive days. During the study, it was found that as we move from day 1 to day 5 the spontaneous alternations of DNP and compound **41** treatment groups at 0.5 mg/kg remained approximately the same. The results indicated that the designed compound **41** is more active, even at half dose, than the marketed drug (DNP) (Figure 4.7). The increased potency of compound **41,** at dose 0.5 mg/kg was due to the multifactorial nature of the compound. The compound showed higher affinity towards MMP-2 and $A\beta_{1-42}$ than the marketed drug. However, the mean number of arm entries remained unchanged across all the experimental groups indicating that the general locomotor activity was not hampered by $A\beta_{1-42}$ toxicity (Figure 4.8). Thus, $A\beta_{1-42}$ impaired hippocampal dependent working memory stands improved upon treatment with compound **41**.

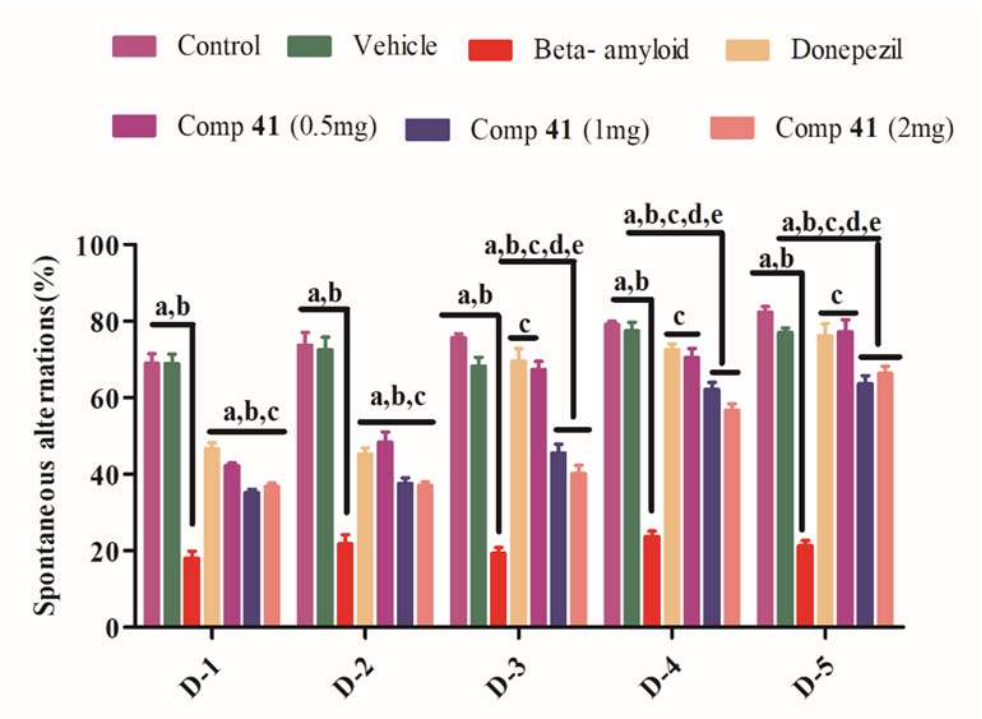

Figure 4.7 Test compound 41 at dose of 0.5 mg/kg improved immediate working memory in rats which received icv injection of $A\beta_{1-42}$ in Y maze test: (A) percentage of spontaneous alterations. Data are expressed as mean ± SEM (n = 6): (a) $p < 0.05$ compared to control (b) $p < 0.05$ compared to vehicle, (c) $p < 0.05$ compared to β amyloid (d) $p < 0.05$ compared to Donepezil, (e) $p < 0.05$ compared to Test compound A 0.5mg, (f) $p < 0.05$ compared to Test compound A 1 mg . [Repeated measure two-way ANOVA followed by Bonferroni test for percentage spontaneous alternations in novel arm entries.

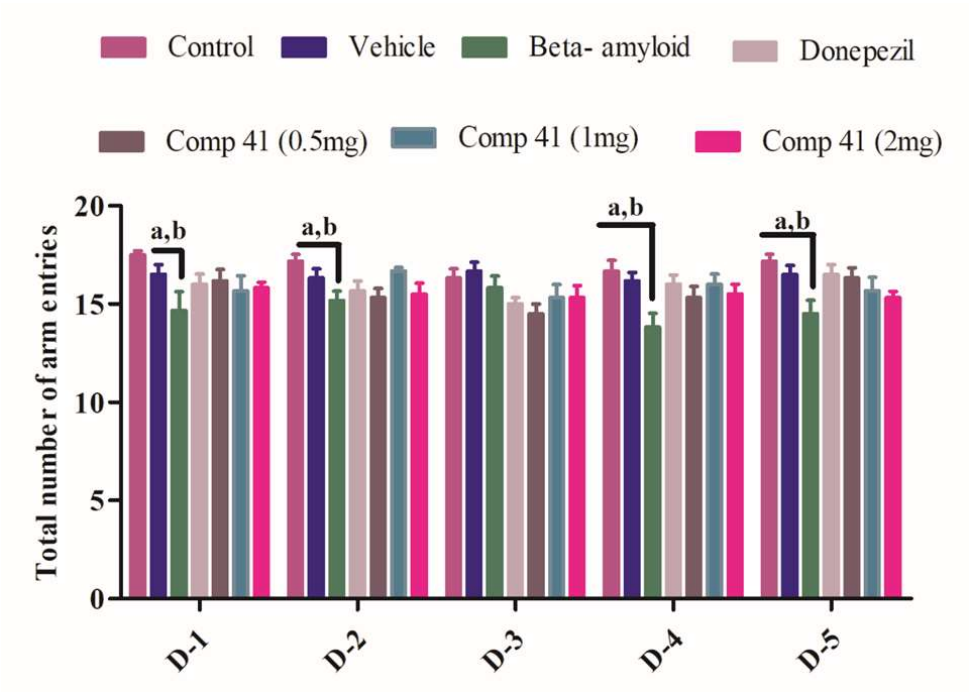

Figure 4.8 Test compound 41 at dose of 0.5 mg/kg improved immediate working memory in rats which received icv injection of $A\beta_{1-42}$ in Y maze test: total number of arm entries, as recorded by an ANY mazeTM (version-3.72, USA) video tracking system. Data are expressed as mean ± SEM (n = 6): (a) $p < 0.05$ compared to control (b) $p < 0.05$ compared to vehicle, (c) $p < 0.05$ compared to β amyloid (d) $p < 0.05$ compared to DNP, (e) $p < 0.05$ compared to Test compound A 0.5mg, (f) $p < 0.05$ compared to Test compound A 1 mg . [Repeated measure two-way ANOVA followed by Bonferroni test for percentage spontaneous alternations in novel arm entries.

4.3.3.9 Pharmacokinetic Studies

Pharmacokinetic studies were performed to evaluate the penetration and localization of compound **41** in brain and hippocampus. Peak plasma concentration was attained after thirty min of dosing and its half-life was found to be 4.93 h. Hippocampus is the center of the memory and learning process thus, localization of the compound in this region was evaluated, which was 0.02 µg/mg in 100X30 mm dimension. Presence of the compound in hippocampus at such concentration established its suitability in the management of neurodegenerative diseases. Log

BB value is generally used for the determination of brain permeability of the drugs [95]. Log BB≥ -1 are considered as acceptable for crossing the blood brain barrier (BBB) [96]. Compound **41** showed log BB value of -0.69 which was suitable for crossing BBB (Table 4.3).

Table 4.3 Pharmacokinetic studies of compound 41 (concentration of compound in plasma, brain and hippocampus after 30 min of dosing.)

Pharmacokinetic parameters	**Extravascular**
Plasma	151.79 µg/mL
Brain	30.64 µg/g
Hippocampus[a]	0.02 µg/mg
Log BB[b]	-0.69
AUC_{0-t}	526.18 µg/mL *h
$AUC_{0-\infty}$	724.27 µg/mL *h
C_{max}	78.55 µg/mL
T_{max}	2 h
$T_{1/2}$	4.93 h

[a]150 mg of 100X30mm size of dissect pieces was used;

[b]ratio of brain to plasma concentration; [c]Value determined for the period of 15 to 240 min.

4.3.4 In-silico studies

4.3.4.1 Molecular docking

The binding energy of compounds 41 and 42, with AChE (PDB ID: 4EY7) was found to be -11.32 and -10. 24 Kcal/mole respectively. The docking study of compound 42 showed π- π interaction with the peripheral anionic site residues Trp286, esteratic locus His447, as well as other residues such as Try337, Phe338. Further, the carbonyl group of the amide showed hydrogen bonding with Try124. The biphenyl sulfonyl group displayed interactions with the various residues of ω-loop i.e. π-alkyl interactions with Leu289, Val294 and hydrogen bonding with Phe295. Compound 41 also showed interactions with ω-loop i.e. π- alkyl interaction with

Leu289, Val294 and hydrogen bonding with Phe295. Try124 and Tyr337 also showed hydrogen bond interactions with quinoline (Figure 9).

The docking of compounds **41** and **42** with MMP-2 (PDB id -1HOV) showed binding energies of -9.25 and -9.46 Kcal/mole respectively. Compound **41** showed π- π interaction with the active site residues Tyr2242, His120, π- alkyl interaction with leu137 and π- sulfur interaction with Tyr142 (supplementary Figure 9). Compound **42** showed π- π interaction with Tyr142, π- alkyl interaction with Leu116, Leu 137 and hydrogen bonding with Ala86, Glu 121. The docking of compound **41** with $A\beta_{1-42}$ (PDB ID: 1ITY) revealed the key interactions of the compound with hydrophobic residues i.e. π- alkyl interaction with Leu17, Ala21, Val24, Lys28, π-σ interaction with Leu17, Ala21 and π-sulphur interaction with Phe20. Binding energy of the synthesized compounds against AChE, MMP-2 and $A\beta_{1-42}$ are reported in Table 2. The field-based QSAR model developed for AChE inhibition showed R^2 of 0.968 and SD of 0.11, while MMP-2 inhibition showed R^2 of 0.972 and SD of 0.053. The number of PLS factors were kept at 2 in order to avoid over-fit models. Further, scatter plot was generated to correlate the observed and predicted activity of the data set. Representation of fields was displayed as contour maps. Scatter plots of QSAR have been included in Figure 4.10.

The compound **41** also showed acceptable ADME profile in *in silico* predictions with *in vitro* Caco-2 cell permeability (Human colorectal carcinoma) value at 10.29 nm/sec, *in vitro* MDCK cell permeability (Mandin Darby Canine Kidney) at 0.073 nm/sec and Percentage predicted human intestinal absorption (HIA, %) at 96.61 which was carried out using PreADMET server and was found to be within acceptable reference limits.

Table 4.4 Binding energies of the compounds docked against the three different targets

Comp_id	Binding energy (Kcal/mole)		
	AChE	MMP2	Aβ
31	-9.04	-9.53	-4.58
32	-9.18	-9.37	-4.66
33	-9.23	-9.02	-5.35
34	-11.1	-8.91	-5.77
35	-10.15	-8.69	-4.86
36	-10.67	-9.09	-4.62
37	-8.68	-7.8	-4.07
38	-10.14	-9.52	-4.96
39	-10.86	-9.84	-5.29
40	-10.08	-9.44	-4.45
41	-11.32	-9.25	-4.26
42	-10.24	-9.46	-4.83
43	-11.51	-9.58	-4.68
44	-10.75	-9.59	-4.54
45	-10.31	-9.17	-4.54
46	-9.96	-9.33	-4.41
DNP	-12.41	-9.29	-5.59

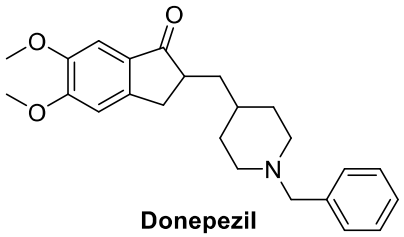

Donepezil
AChE =-12.41
MMP2 = -9.29
Aβ = -5.59

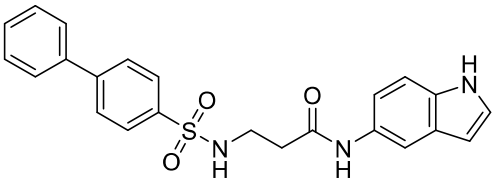

Compound 45
AChE = -10.31
MMP2 = -9.17
Aβ = -4.54

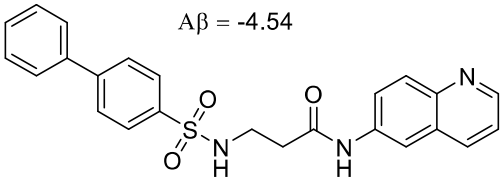

Compound 43
AChE = -11.51
MMP2 = -9.58
Aβ = -4.68

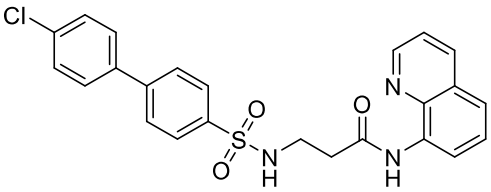

Compound 41
AChE = -11.32
MMP2 = -9.25
Aβ = -4.26

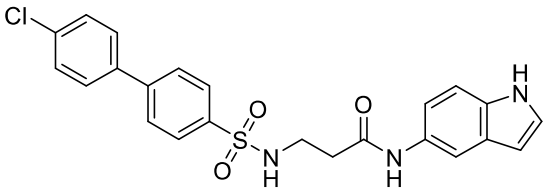

Compound 46
AChE = -9.96
MMP2 = -9.33
Aβ = -4.41

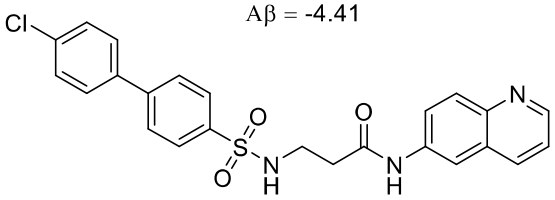

Compound 44
AChE = -10.75
MMP2 = -9.59
Aβ = -4.54

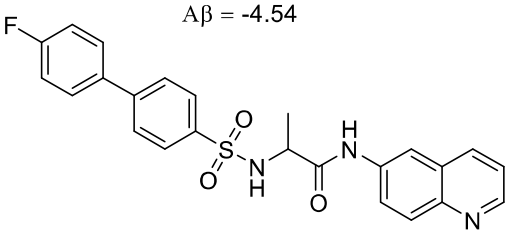

Compound 42
AChE = -10.24
MMP2 = -9.46
Aβ = -4.83

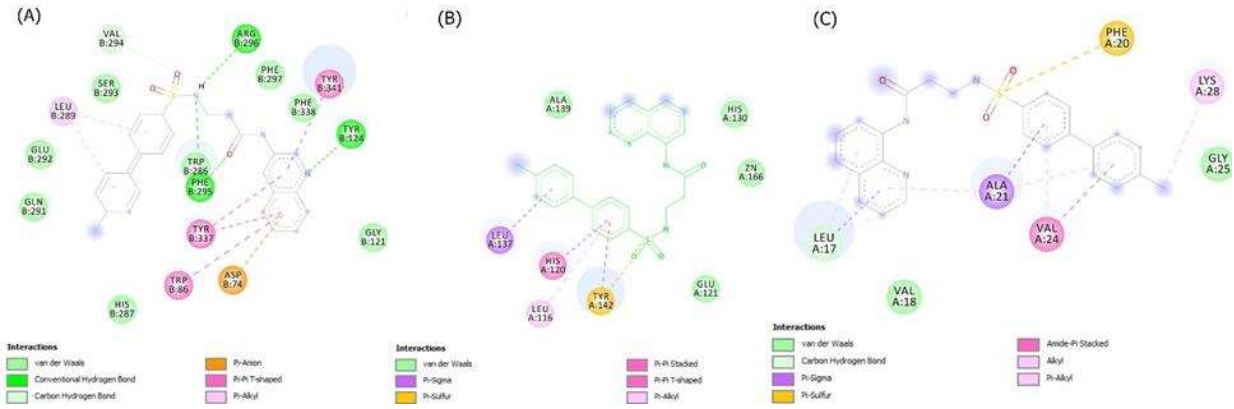

Figure 4.9 Compounds with the highest binding energies followed by docking poses of compound 41 against (A) AChE (PDB ID:- 4EY7), (B) MMP-2 (PDB ID: 1HOB) and (C) $A\beta_{1-42}$ (PDB id.- 1ITY).

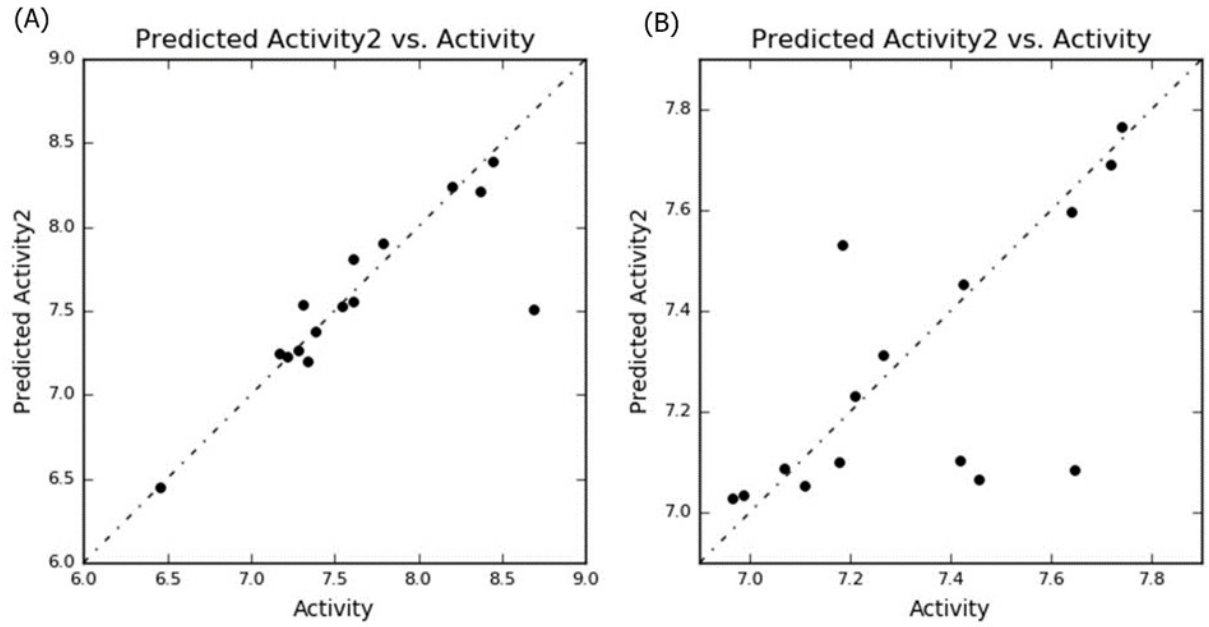

Figure 4.10 Scattered plot of the predicted v/s observed activity of (A) AChE and (B) MMP-2

4.4 Conclusions

Quinoline derivatives were found to be superior to that of the indole derivatives *vis-à-vis* the selected parameters. Quinolines, substituted at the position 8 showed better activity compared to the derivatives substituted at the positions 6 and 3. Compound **41**, substituted at positon 8, emerged as the lead molecule. The study also revealed that biphenyl containing compounds had better MMP-2, AChE and BChE inhibition potential than monophenyl analogues. The *in-vitro* inhibition studies i.e., AChE (IC_{50} 4.28±0.15 μM), BChE (IC_{50} 1.32±0.02 μM), MMP-2 (IC_{50} 18.24 ±1.62 nM) of the compound established its potency whereas, the inhibition assay of metal induced $A\beta_{1-42}$ aggregation followed by confocal imaging revealed Aβ disaggregation. *In-vivo* experiments indicated that the compound showed comparable cognitive effects with that of the marketed drug (DNP) at half the dose. Also, the general locomotor activity remained unhampered whereas; hippocampal dependent working memory was improved by the compound. The therapeutic potential of compound 41 seems to be due to its multifactorial nature of action. Pharmacokinetic studies of the lead compound further reinforced that it has a decent ADME profile along with the mentioned therapeutic activity.